THESIS FOR THE DEGREE OF DOCTOR OF PHILOSOPHY

Lean NO_x reduction over silver-alumina from lab-scale to real conditions

Effects of reducing agent and catalyst composition

FREDRIK K. GUNNARSSON

Department of Chemical and Biological Engineering

CHALMERS UNIVERSITY OF TECHNOLOGY

Gothenburg, Sweden 2014

CHALMERS
UNIVERSITY OF TECHNOLOGY

Lean NO_x reduction over silver-alumina from lab-scale to real conditions
Effects of reducing agent and catalyst composition

FREDRIK K. GUNNARSSON

ISBN 978-91-7597-061-5

Doktorsavhandling vid Institutionen för kemi- och bioteknik
Chalmers tekniska högskola
Ny serie nr. 3742
ISSN 0346-718X

Applied Surface Chemistry
Department of Chemical and Biological Engineering
Chalmers University of Technology
SE-412 96 Gothenburg
Sweden
Telephone + 46 (0)31-772 1000

Chalmers Reproservice
Gothenburg, Sweden 2014

Lean NO_x reduction over silver-alumina from lab-scale to real conditions
Effects of reducing agent and catalyst composition

FREDRIK GUNNARSSON

Applied surface chemistry
Department of Chemical and Biological Engineering
Chalmers University of Technology

Abstract

The focus of this work is to increase the understanding of lean NO_x reduction over silver-alumina catalysts using hydrocarbons as the reducing agent (HC-SCR), in particular by investigating the effect of silver loading, the role of platinum doping, and the effect of the type of reducing agent. In addition, the effects of aging and hydrothermal treatment on the catalytic activity and selectivity, and the influence of real engine exhausts were investigated, with special attention to the low-temperature activity. Silver-alumina samples were prepared using a sol-gel method, including freeze-drying, and evaluated for HC-SCR. The samples were synthesized with varying silver loading, with and without addition of trace amounts of platinum. NO_x reduction activity studies, hydrothermal treatment and oxidation experiments were performed in a synthetic gas bench reactor using model hydrocarbons (n-octane, ethane, ethene, ethyne) and commercially available biofuels (NExBTL, ethanol) as the reducing agent. The samples were characterized with respect to surface area (BET) as well as the type and relative amount of surface silver species (UV-vis, XPS). An optimized catalyst was also up-scaled and investigated in an engine bench reactor, with diesel exhausts, using a commercial biofuel as reducing agent, and with hydrogen supplied via a reformer catalyst.

The results show that silver-alumina catalysts, prepared via sol-gel synthesis, display a high consistency regarding surface area and the relative amount of different silver species, as the silver loading is varied. Furthermore, it can be observed that activation for hydrocarbon oxidation generally proceeds more easily with increasing bond order of the hydrocarbon. For instance, the use of hydrocarbons with high bond order, *e.g.* ethyne, as reductant for NO_x, results not only in the highest peak activity for lean NO_x reduction but also in considerable high activity in a wide temperature range mainly thanks to increased activity at low temperatures compared to a corresponding hydrocarbon with lower bond order. With increasing silver loading, the oxidation reactions are favored such that both the hydrocarbon and the NO activation occur at lower temperatures. This is also corroborated by experiments with oxidized hydrocarbons (ethanol) displaying a complete reduction of NO_x over a wide temperature range. As the hydrocarbon chain-length is increased, the NO_x reduction decreases, however, high activity can be seen even when using the commercial biodiesel, with a reduction of over 70 % in laboratory scale experiments.

Furthermore, it is concluded that as the samples are doped with trace-amounts of platinum, the activity for lean NO_x reduction at low temperatures is enhanced when using n-octane. The catalyst composition showing the highest activity for NO_x reduction, using n-octane as reducing agent, is found to be a 2 wt. % Ag/Al_2O_3 sample doped with 500 ppm platinum. This catalyst also displays the highest low-temperature activity, most likely owing to an increased ability to partially oxidize the

hydrocarbon reductant as well as higher adsorption of the hydrocarbon on the surface, attributed to the Pt doping. The 4 wt. % Ag/Al_2O_3 sample doped with 100 ppm platinum shows high activity in close to real conditions with the addition of reformate. It can also be concluded that adding reformate instead of pure hydrogen, to the same H_2 concentration, results in an equal or even higher activity for NO_x reduction, likely owing to the presence of unreacted hydrocarbons in the reformate.

In conclusion this work shows HC-SCR as a viable concept for NO_x reduction, even though many challenges remain. Low-level platinum doping is shown to increase the activity for NO_x reduction, especially at low temperatures and for higher hydrocarbons. In addition, the in-house synthesized catalysts are compatible with commercial biofuels for both heavy-duty (NExBTL) and light-duty (ethanol) vehicles. The real engine experiments also show a promising NO_x reduction, both when using pure hydrogen and reformate.

Keywords: Lean NO_x reduction, HC-SCR, Ag/Al_2O_3, biofuels, ethanol, Pt-doping, catalyst ageing, low-temperature activity

List of Publications

This thesis is based on the following publications, I-V:

I. Improved low-temperature activity of silver-alumina for lean NO_x reduction – Effects of Ag loading and low-level Pt doping

Fredrik Gunnarsson, Hannes Kannisto, Magnus Skoglundh and Hanna Härelind

Applied Catalysis B: Environmental 152-153 (2014) 218-225

II. Influence of ageing, silver loading and type of reducing agent on the lean NO_x reduction over Ag-Al_2O_3 catalysts

Fredrik Gunnarsson, Jenny-Yue Zheng, Hannes Kannisto, Clément Cid, Anna Lindholm, Miroslawa Milh, Magnus Skoglundh and Hanna Härelind

Topics in Catalysis, 56 (2013) 416-420

III. Influence of the carbon–carbon bond order and silver loading on the formation of surface species and gas phase oxidation products in absence and presence of NO_x over silver-alumina catalysts

Hanna Härelind, Fredrik Gunnarsson, Seyyed Majid Sharif Vaghefi, Magnus Skoglundh and Per-Anders Carlsson.

ACS Catalysis, 2 (2012) 1615-1623

IV. NO_x reduction over Ag/Al_2O_3 catalysts via EtOH-SCR using ethanol/gasoline blends

Fredrik Gunnarsson, Josh Pihl, Todd Toops, Magnus Skoglundh and Hanna Härelind.

Manuscript

V. Combining HC-SCR over Ag/Al_2O_3 and hydrogen generation over Rh/CeO_2-ZrO_2 using biofuels: An integrated system approach for real applications

Fredrik Gunnarsson, Moa Z. Granlund, Mattias Englund, Jazaer Dawody, Lars J. Pettersson and Hanna Härelind.

Applied Catalysis B: Environmental 162 (2015) 583-592

The results covered in this thesis were also presented at the following conferences:

I. *Optimizing feed concentrations for lean NO_x reduction by HC-SCR over Ag/Al_2O_3*
F. Gunnarsson, H. Kannisto and H.H. Ingelsten
Poster presentation
14th Nordic Symposium on Catalysis, 29-31/8, 2010, Helsingør, Denmark

II. *The influence of trace-amount PM-doping on lean NO_x reduction by HC-SCR over Ag/Al_2O_3*
F. Gunnarsson, H. Kannisto and H.H. Ingelsten
Poster presentation
22nd North American Catalysis Society Meeting, 5-10/6, 2011, Detroit, USA

III. *Influence of silver loading and type of reducing agent on the lean NO_x reduction over $Ag\text{-}Al_2O_3$ catalysts*
F. Gunnarsson, J.-Y. Zheng, H. Kannisto, C. Cid, A. Lindholm, M. Milh, M. Skoglundh and H. Härelind
Poster presentation
9th International Congress on Catalysis and Automotive Pollution Control, 29-31/8, 2012, Brussels, Belgium

IV. *Improved low-temperature activity of silver-alumina for lean NO_x reduction – effects of Ag loading and low level Pt doping*
F. Gunnarsson, H. Kannisto, M. Skoglundh and H.H. Ingelsten
Oral presentation
Cross-cut Lean Exhaust Emission Reduction Simulations, 29/4-1/5, 2013, Dearborn, USA

V. *Improved low-temperature activity of Ag-alumina for lean NO_x reduction – effects of Ag loading and low-level Pt doping*
F. Gunnarsson, H. Kannisto, M. Skoglundh and H.H. Ingelsten
Poster presentation
23rd North American Catalysis Society Meeting, 3-7/6, 2013, Louisville, USA

VI. *Combining HC-SCR over Ag/Al_2O_3 and hydrogen generation over $Rh/CeO_2\text{-}ZrO_2$ using bio-fuels: an integrated system approach for real applications*
F. Gunnarsson, M. Z. Granlund, M. Englund, J. Dawody, L. J. Pettersson and H. Härelind
Oral presentation
16th Nordic Symposium on Catalysis, 15-17/7, 2014, Oslo, Norway

Contribution report

I. Responsible for all experimental and analytical work as well as writing of the manuscript.

II. Responsible for the experimental work and analysis regarding the reducing agent and hydrothermal treatment study as well as writing of the manuscript.

III. Responsible for flow-reactor experiments and catalyst synthesis. Taking part in writing of the manuscript together with my co-authors.

IV. Responsible for the synthesis of the catalysts, experimental work and analysis of data as well as writing of the manuscript.

V. The paper was co-authored with Moa Ziethén-Granlund. The work was distributed equally between us and we both contributed equally to the experimental work, the evaluation and writing of the manuscript.

Table of Contents

1. List of abbreviations

AdBlue	Urea-solution (Europe) (32% urea in water)
A/F	Air-to-fuel ratio
BE	Binding energy
BET	Brunauer-Emmet-Teller, method for determening SSA
CEM	Controlled evaporator mixer
C/N	Carbon-to-nitrogen ratio
DEF	Diesel exhaust fluid (US) (32% urea in water)
DOC	Diesel oxidation catalyst
DPF	Diesel particulate filter
DRIFTS	Diffuse reflectance infrared Fourier transformed spectroscopy
EGR	Exhaust gas recirculation
EtOH	Ethanol
FTIR	Fourier transformed infrared spectroscopy
GHSV	Gas hourly space velocity, h^{-1}
HC	Hydrocarbon
HT	Hydrothermally
ID	Inner diameter
L	Length
MeOH	Methanol
MK1	Environmental class 1 (Miljöklass 1)
MS	Mass spectrometry
NO_x	Nitrogen oxides ($NO+NO_2$)
OD	Outer diameter
PGM	Platinum group metals
PSR	Pilot-scale reactor

SCR	Selective catalytic reduction
SGB	Synthetic gas bench
SS	Steady-state
SSA	Specific surface area, m^2/g
TWC	Three-way catalyst
UV-vis	Ultraviolet-visual spectroscopy
XPS	X-ray photoelectron spectroscopy

2. Introduction

As the market becomes increasingly more globalized, the need for transports has increased steadily over the last century. In 1990 the number of cars, motorcycles, busses and trucks in the world was estimated to 650 million [1]. Although extensive research is performed to find alternatives, the combustion engine will most likely be the dominant system for automotive propulsion during the coming decennia. Due to the significant impact from the combustion engine on the environment, ever more stringent emission legislation has been implemented regarding both the emissions of carbon dioxide (CO_2), as well as the emissions of more directly harmful gases, *i.e.* carbon monoxide (CO), nitrogen oxides (NO_x), particulate matter and unburned fuel [2, 3]. These emission legislations and the limited resources of fossil fuels are strong drivers for energy-efficient engine concepts, such as diesel and lean-burn engines [4], which reduce the fuel consumption and thereby also the emissions of CO_2 as compared to stoichiometric gasoline engines. Emissions of NO_x are hazardous to the environment, acting as a source to ground level ozone, acid rain and eutrophication, as well as being directly harmful to humans. The legislated emission levels of NO_x for heavy-duty vehicles have decreased from 8.0 g/kWh in Euro I (1992), to 0.4 g/kWh in Euro VI (2014) (Fig. 1) [4]. Solving the problem of NO_x emission abatement is therefore of crucial importance. The conventional way of reducing NO_x emissions has been by the use of a three-way catalyst (TWC). The catalyst consists of noble metals (platinum, palladium and rhodium) supported on alumina (γ-Al_2O_3) and ceria (CeO_2), and has the ability to simultaneously oxidize CO and unburned hydrocarbons while also reducing the NO_x. However, the lean environment in the exhaust gas from new engine systems, with high air-to-fuel ratios, obstructs the NO_x reduction in the TWC, which needs to operate closer to stoichiometric air-to-fuel ratio (A/F= 14.7) [5]. As a result of the increased combustion efficiency *i.e.* increased air-to-fuel ratio, the new engine systems also operate at much lower temperatures, resulting in exhaust temperatures as low as 150°C. This also introduces a true challenge when designing alternative catalytic techniques.

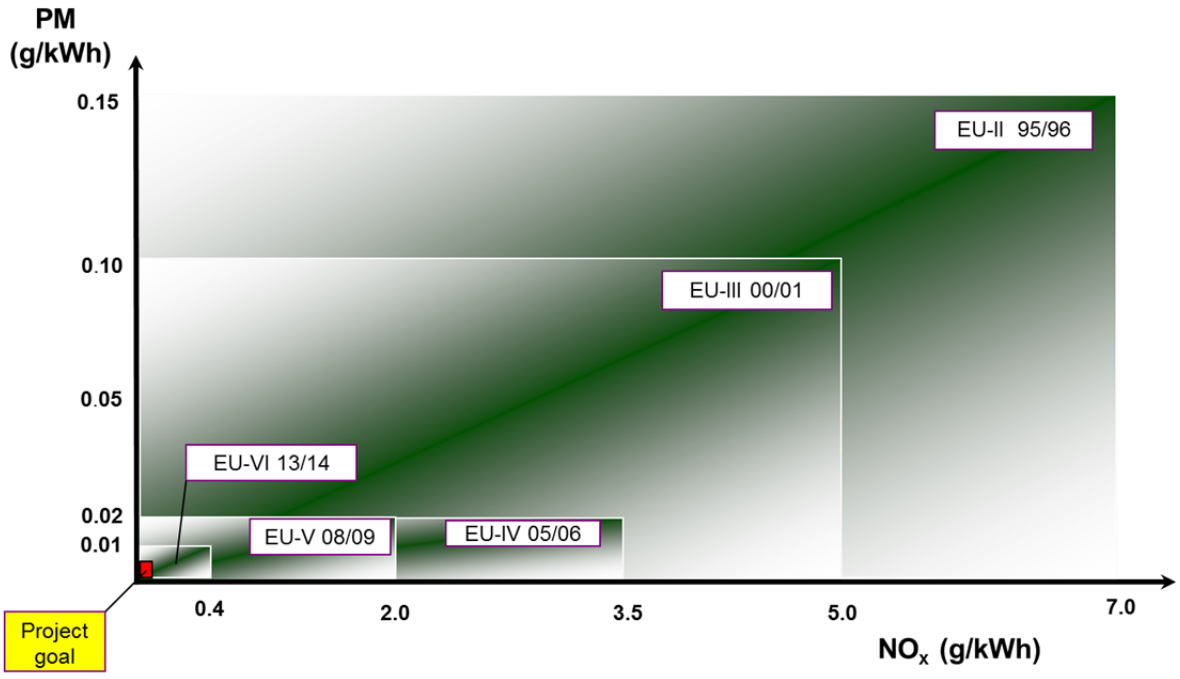

Figure 1: Progression of emission legislation in Europe for trucks and busses (EURO II-VI).

A number of new techniques have been developed in order to decrease the emission of NO_x from combustion engines. One example is exhaust gas recirculation (EGR) were the inlet air to the combustion chamber is mixed with exhaust gases, lowering the oxygen concentration in the combustion chamber and thereby lowering the amount of formed NO_x [6]. Other techniques are NO_x storage catalysts were the engine is run at alternating lean and rich phases, storing NO_x during the lean phase and then reducing the stored NO_x during the shorter rich phase [5, 7-9] and selective catalytic reduction (SCR), using either hydrocarbons or ammonia from urea as reducing agent. The focus of this thesis is selective catalytic reduction of NO_x over silver alumina catalysts using hydrocarbons, *i.e.* fuel, (HC-SCR), as the reducing agent.

2.1. Biofuels

For the past century the consumption of energy has increased drastically with the main energy production deriving from fossil sources. These may be in the form of brown coal, used in power plants for electricity generation or oil based products such as diesel, gasoline etc. As these sources are finite, concerns regarding the availability of such energy sources have grown. The number of new oil reservoirs that are discovered annually is decreasing and although the oil companies still find new reservoirs, they tend to be in areas where increasingly more difficult extraction methods are required.

In the year 1988, the International Panel on Climate Change (IPCC) was formed with the goal: "…stabilization of greenhouse gas concentrations in the atmosphere at a level that would prevent dangerous anthropogenic interference with the climate system…" [10]. The committee has since then produced a number of reports based on publications from a multitude of research groups. The absolute majority have come to the conclusion that the addition of anthropogenic CO_2 is the main cause of global warming. Mathematical models predict a rise of the ocean levels, an increase in extreme weather phenomena and the disappearance of natural habitats, crucial for the survival of many endangered animals [11, 12]. Many different strategies have been proposed, but the main goal for all of them is to reduce the use of fossil fuels.

In order to ensure a high mobility for future generations, alternative sources for energy to the transport sector is crucial. Many alternatives to fossil fuels have been suggested and implemented, with the first mass produced cars running on ethanol reaching the market in 1979. Other techniques like the Fisher-Tropsch (F-T) process [13, 14], used already in Germany during the Second World War to produce synthetic diesel, is based on the reconstruction of carbon monoxide and hydrogen (syngas) into long-chained liquid hydrocarbons via a catalyzed reaction. Franz Fisher and Hans Tropsch developed the F-T process in 1925. The source for the base chemicals needed for the production of Fisher-Tropsch diesel can vary from coal, used in Germany in the 30's and 40's, to syngas produced from biomass *e.g.* waste food, lumber by-products etc. making it a very versatile fuel [14-16]. The production process does however require a catalyst, and although research for improvement of such catalysts continues to this date, many challenges still remain, *e.g.* selectivity problems and price of the catalyst. As a result, F-T diesel is still not in a price range that can compete with fossil fuels.

Other alternatives to fossil fuels are short-chained liquid hydrocarbons *e.g.* methanol (MeOH), ethanol (EtOH), biomass-to-liquid fuels (BLT) and dimethyl ether (DME), all with advantages and drawbacks [17-22]. Ethanol and BLT-fuels have been the focus as alternative fuels in this thesis, with EtOH mainly being suitable for light-duty vehicles and BTL for heavy-duty, due to the difference in energy density. The first car, produced by Ford in 1896, was intended to run on ethanol, however as

a result of the fossil fuels being so much cheaper during this period, the ethanol cars were simply too expensive to drive. Many countries have a mixture of 10 % ethanol and 90 % petrol (E10) as a standard today [23, 24]. In an attempt to further reduce the emissions of anthropogenic CO_2, legislators are planning an increase of the ethanol content from 10 % to 15 % (E15). Cars running on ethanol as the main fuel returned to the market in 1979, as a response to the oil crisis, with the introduction of E85 in many countries, and in some cases even higher ethanol blends have been introduced *e.g.* E93 in Brazil with 7% H_2O [25]. The actual environmental gain of switching from petrol to EtOH is however not as large as one initially might think. The majority of all EtOH is produced by fermentation of sugar rich feed stock, such as corn and sugar cane, with a fermentation process reaching approximately 10 % EtOH. In order to achieve higher concentration the finished fermentation product requires distillation, a very energy consuming process. The crops needed for the fermentation process also require maintenance, pesticides, harvesting and separation, all of which are energy consuming steps. Issues have also been raised concerning the usage of fertile lands to manufacture fuels as opposed to the production of food [26, 27].

The technique of producing liquid fuels via biomass-to-liquid is a promising alternative to fossil fuels. Although various techniques exist, producing fuels from waste oil is promising, as it would not compete with other markets and as no distillation is required, the process can be made very efficient. Currently, due to lack of infrastructure for recycled waste oils, the process utilizes palm oil as the main raw material, however with increased awareness and potential legislation the finished product can eventually become CO_2 neutral.

2.2. Objectives

The objective of this work is to increase the understanding of the catalytic processes concerning the lean NO_x reduction over silver-alumina catalysts. The work ranges from synthesis and characterization to activity measurements, both in model scale and engine bench scale. In particular, the effect of silver loading, the role of platinum-doping, and the effects of aging and hydrothermal treatment on the catalytic activity, selectivity and low-temperature performance are in focus. In addition, the study includes the effect of the reducing agent, model hydrocarbons as well as commercially available biofuels.

The project was performed as part of the second phase of the Mistra project E4, Energy Efficient Reduction of Exhaust Emissions from Vehicles. The overall goal of the Mistra E4 project is the reduction of NO_x and PM, without increasing the emission of CO_2. The second phase of the Mistra E4 project aims to further improve the applied technologies and secure the functionality and stability of the integrated system. Utilization of suitable renewable fuels as alternatives to fossil fuels to decrease the emission of anthropogenic CO_2 is also a key element.

3. Selective Catalytic Reduction

Selective catalytic reduction of NO_x is a promising technique to reduce NO_x at high air-to-fuel ratios, for which the TWC lacks in performance. The urea-SCR technique is already implemented in large parts of the industrialized world, both in the automotive sector and for stationary applications. However, although urea solutions for the automotive industry, *e.g.* AdBlue and DEF, are readily available in many countries, *e.g.* USA and large parts of Europe, access to urea is still very limited in the larger part of the world [28]. As the HC-SCR system uses the fuel as the reducing agent, no need for additional components exists and the system can be utilized for all vehicles world-wide, giving it a great advantage. The concept of selectively reducing NO_x using hydrocarbon as the reducing agent was first introduced in 1990 by Iwamoto *et al.* [29] and Held *et al.* [30], both independently showing that the presence of hydrocarbons enhanced the lean NO_x reduction over Cu-ZSM5 catalysts. These catalysts were however found to be sensitive to water. Subsequently, catalysts with higher tolerance to hydrothermal conditions were investigated, which is discussed in detail by Burch [31]. In 1993, Miyadere showed very high activity for NO_x reduction, as compared to previous studies, over silver supported on alumina in the presence of water [32]. The Ag-alumina system is described in section 3.1.

The main reactions in HC-SCR are the NO_x reduction, facilitated by the hydrocarbon reductant, and the competing combustion reaction, where the hydrocarbon is oxidized to CO_2 by the excess oxygen. The NO_x reduction reaction is divided into three main reactions: I) the oxidation of NO to NO_2 and the formation of surface nitrates and nitrites, II) the adsorption of hydrocarbons onto the surface and the partial oxidation of the hydrocarbons forming various oxygenated carbon surface species and III) the reaction between the partially oxidized hydrocarbons and the surface nitrogen containing species, forming N_2, CO_2 and water [31].

One of the main steps, thought to be crucial for achieving high performance at low temperature, is the activation of the hydrocarbon, *i.e.* the partial oxidation, before it reacts with the NO_x to form N_2 [33, 34]. Burch *et al.* [35] and Arve *et al*. [36] have proposed that the initial step in hydrocarbon activation is the dissociation of the first hydrogen from the hydrocarbon reductant. The dissociation is related to the sticking probability, *i.e.* hydrocarbon-surface interaction, which is proportionally dependent on the sticking coefficient and exponentially dependent on the dissociative chemisorption energy of the molecule on the surface [1]. The oxidation properties of the active phase and the dissociative chemisorption energy for the hydrocarbon on the surface are therefore of crucial importance and need to be tuned so that only partial oxidation takes place, without totally combusting the hydrocarbon.

3.1. The silver alumina system

Silver-alumina (Ag/Al_2O_3) has been pointed out as a potential catalyst for lean NO_x reduction, displaying promising results for a variety of hydrocarbons, including fossil fuels and biofuels [37-42]. One drawback with the Ag/Al_2O_3 system has been that the system requires relatively high temperatures to achieve high activity, while as the energy efficiency in engines increases, the exhaust gas temperature decreases. Many new engine designs also include heat recovery systems, which decrease the exhaust gas temperature in the catalyst even further. Nevertheless, the active temperature window for HC-SCR over Ag/Al_2O_3 may be shifted towards lower temperatures, provided a small amount of hydrogen is introduced to the exhaust feed [43-46]. The addition of hydrogen further results in an over-all increase in the NO_x reduction. This phenomenon is referred to

as the hydrogen effect, described below. The 2 wt. % Ag/Al_2O_3 system has shown high NO_x reduction activity in the presence of hydrogen [32, 39, 46-48]. The added hydrogen does however increase the fuel-penalty. Recently Kannisto *et al.* have showed that hydrogen levels as low as 1000 ppm, produced from onboard fuel-reforming, result in a fuel penalty of about 2% (reducing agent + H_2 addition) [49], cf. 0.5% for urea-SCR.

As mentioned previously, the main reactions in HC-SCR are the NO_x reduction, by the hydrocarbon, and the competing reaction where the hydrocarbon is oxidized by the oxygen, *i.e.* combusted. To favor the desired reduction reaction and to reach a good low-temperature performance, the hydrocarbon needs to be activated, *i.e.* partially oxidized, before reacting with the NO_x [33-37]. This can be achieved by various routes, likely including several active sites. Although the complete reaction mechanism over Ag/Al_2O_3 is still under debate, several active sites are likely involved *e.g.* silver ions, small silver clusters and larger metallic silver particles [50-52]. It has for instance been suggested that $Ag_n^{\delta+}$ clusters are highly active for the HC-SCR process [53], particularly for the activation of the reducing agent by partial oxidation. It has been shown that very small silver clusters (Ag_n<8) to a greater extent provide active sites for lean NO_x reduction with hydrocarbons as compared to larger, more metal like, silver particles Furthermore, it has been shown that different forms of oxidized silver species, like Ag^+, Ag_2O, or silver aluminate, favor the reduction of NO to N_2 [54, 55] whereas metallic silver particles are more active for oxidation reactions [56-58]. These findings indicate that catalysts, that are active for NO_x reduction by hydrocarbons most likely contain highly dispersed ionic, oxidized and/or $Ag_n^{\delta+}$ silver species. To prevent the competing total combustion reaction of hydrocarbon to CO_2 and H_2O, the oxidation strength of the oxidation sites is of crucial importance, ensuring that the hydrocarbon is only partially oxidized to active surface species.

Ways to facilitate the partial oxidation of the hydrocarbon may be to incorporate additional oxidation sites in the Ag-alumina catalyst or by altering the oxidizing potential of the existing oxidation sites. Previous studies [49] indicate that trace-amounts of platinum incorporated in the silver-alumina catalyst, increase the maximum NO_x reduction and at the same time decrease the onset temperature of the HC-SCR reaction. The study suggests that platinum acts as an oxidizing agent, facilitating partial oxidation of the hydrocarbon and making it more readily available for the NO_x reduction reaction. The authors do however stress that, as platinum is such a strong oxidizing agent, it is important to keep a low platinum level to reduce the risk of combusting the reducing agent. It has also been proposed that the addition of platinum chloride increases the adsorption of hydrocarbons, which could facilitate a higher NO_x reduction activity at low temperature since more hydrocarbons would be available on the surface [59]. The authors ascribe the increase in HC-adsorption to a change in the acidity of the surface due to chlorine residue from the synthesis.

As stated previously, the addition of hydrogen to the exhaust feed will improve both the activity of NO_x reduction, and lower the operating temperature window, for HC-SCR over Ag/Al_2O_3 catalysts. This effect was first discovered in the year 2000 by Satokawa *et al*. [43] and resulted in increased interest for the Ag/Al_2O_3 catalysts system. The effect has since then been confirmed, for various hydrocarbons, and the underlying properties of the effect has been investigated thoroughly, *e.g.* [39, 60-62]. The increase in activity can be seen almost instantaneously on the addition of hydrogen and disappears as hydrogen is removed from the feed, with very sharp steps in the reduction curve. The effect does not change over time and the improved activity can be achieved over and over again

when performing pulse experiments. Hydrogen is however not active as a reductant by itself, but rather as a promoter for the hydrocarbon reductant [60, 61]. Although extensive studies on the hydrogen effect have been performed, since its discovery, the underlying phenomena behind the effect are still under debate. The studies discuss *e.g.* changes in the silver configuration and chemical state [45, 62, 63], promotion of the partial oxidation of the hydrocarbon [46, 48, 54], and the removal of inactive surface species which may inhibit the desired reactions [39, 42, 54, 62, 64].

3.2. Deactivation

As catalysts are not consumed in a reaction, but rather provide an alternative reaction pathway, they should in theory remain in their original state also after the reaction has taken place, however many factors contribute to the degradation of a catalyst. The degradation processes are divided into three major mechanisms: poisoning, fouling and thermal degradation [65]. Poisoning occurs when a material binds strongly to the active sites of a catalyst, preventing the reactants from reaching the active site and/or influencing the electronic state of the active site and thereby inhibiting the catalytic processes. Although the poison in some cases can be removed, poisoning is manly an irreversible process. The poisoning component may be a byproduct in the reactant flow or the reactants themselves. The latter is referred to as self-poisoning, were a catalytic surface is saturated with one of the reactants preventing other reactants from adsorbing. An example of this is CO poisoning on platinum based catalysts during CO oxidation [66, 67]. The light-off for such reactions occurs at a higher temperature compared to extinction of the reaction. This is due to a complete coverage of CO on the surface at low temperatures, which prevents oxygen from reaching the surface. At the light-off temperature, enough CO molecules have desorbed from the surface to enable adsorption of oxygen and then further reaction to CO_2. During the extinction process both species are adsorbed on the surface, giving rise to a hysteresis behavior.

Fouling is similar to poisoning, however fouling is usually reversible. Instead of a chemical bond to the active site, a fouling agent physically blocks the surface and the pores, covering the active sites and the active surface area [68, 69]. Catalysts which have been deactivated by fouling can be regenerated both by treating them in reactive gases and by subjecting them to elevated temperatures [70]. Thermal degradation can either be derived from alternating heating and cooling the material, resulting in the formation of cracks in the support material and thereby loss of surface area and active material[71]. High temperatures can also result in sintering of small active particles, which then agglomerate, decreasing the active surface area and thereby the activity of the catalyst [72]. At high enough temperature also the structure of the support material collapses. The tolerance towards deactivation in high temperature environment is therefore of great importance.

3.3. Surface structure and adsorption processes

A key property governing the efficiency of a catalyst is the ability for the reactive species to adsorb onto the surface of the catalyst. During adsorption, the electron density configuration of the molecule will be distorted, facilitating bond breaking and bond formation at lower energy compared to a gas phase reaction. The charge density can in some cases drastically change, facilitating bond breaking of the molecule directly on the surface, *e.g.* H_2 dissociation over Pt (533) sites [73]. The parameters which govern the ability for adsorption are for example the geometry of the molecule,

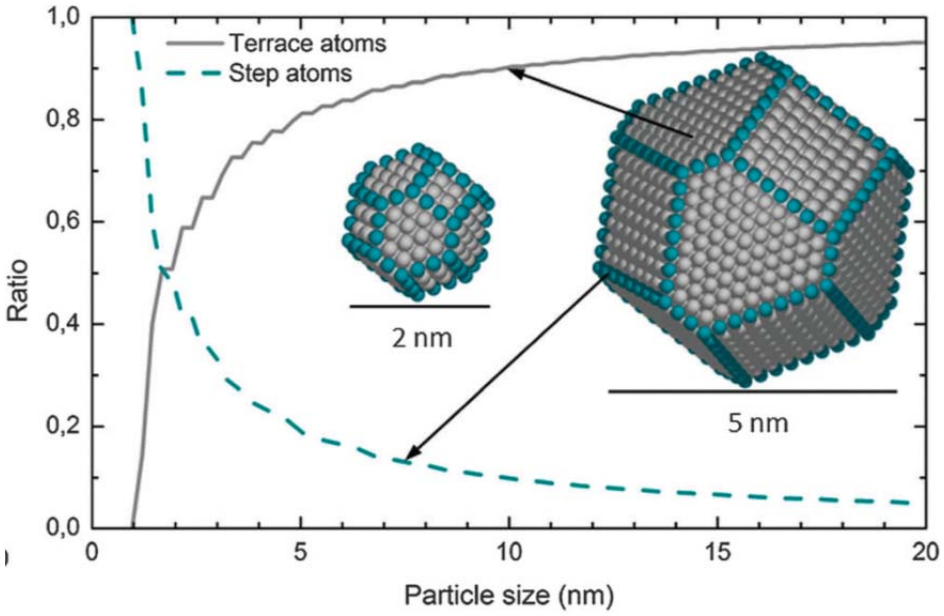

Figure 2: Step vs. terrace atomic ratio as a function of silver particle size. Constructed Wulff shapes for 2 and 5 nm silver particles. Step atoms are highlighted. (Reproduced in part from [52] with permission of The Royal Society of Chemistry.)

the bond order and the edge groups. In addition, the type of surface plays an important role where the surface configuration and material are the main factors. When discussing the different types of active sites on a catalyst surface three main distinctions are made; terrace sites, edge sites and corner sites [1]. Terrace sites are referred to when a molecule adsorbs onto a flat surface, edges can derive from plate displacement on a surface between the corners of a site, such as the edge between the corners on a cube, and the corner sites are the corners themselves. As the active phase cluster grows in size, the valence electrons will become more dislocated, giving the particle a metal-like behavior and the difference in electronic cloud distribution will increase between the terrace, edge and corner sites. For a sufficiently large particle, many sites can be available, *e.g.* when comparing Ag particles the ratio between step and terrace sites, varying as a function of particle size and the sites per particle grows with increasing particle size (Figure 2, Reproduced in part from [52] with permission of The Royal Society of Chemistry). The number of step sites per mass of active metal increases with decreasing particle size. In addition to the geometric shape of the particle, the lattice structure of the particle is also of great importance, *e.g.* CO adsorption on the *p*(4×4) structure of oxidized Ag(111) showing low activation energies for the formation of CO_3^{2-} from CO [74] and CO oxidation over an ultrathin MgO film supported on Ag(100) where the reaction barrier mainly originates from the breaking of the O-O bond *cf.* the CO-Pt and O-Pt bond on a Pt(111) surface [75].

Apart from the structure and geometry, different active phases of the metals will have different affinity for adsorbing the reactive species. Regarding the HC-SCR reaction, Burch *et al.* [35] and Arve *et al*. [36] have proposed that the initial step in hydrocarbon activation, is the abstraction of the first hydrogen from the reductant. The dissociation is related to the sticking probability, which is proportionally dependent on the sticking coefficient and exponentially dependent on the dissociative chemisorption energy of the molecule on the surface [76]. Comparing the dissociation energies for different molecules on *e.g.* silver and platinum surfaces, the dissociation energy is always lower for platinum according to Bligaard *et al.* [77]. The authors report that the dissociative chemisorption for CH_4 on platinum *cf.* silver differs by 6.49 eV [77], which is a substantial difference. Further, the

Brønsted-Evans-Polanyi (BEP) relation [78, 79] states that the change in activation energy follows the change in energy of the final state for the chemically dissociated molecule. The BEP relation has also been verified for metal oxides [76], which ensures that the activation barrier will be lower for the oxidized Pt particles as well, in relation to the oxidized Ag species. The relative sticking probability should thus be higher over the Pt species than for the corresponding Ag species in our samples.

4. Experimental methods

All studies have been performed on in-house synthesized Ag/Al_2O_3 catalysts, prepared via sol-gel synthesis, with various silver loading and Pt doping. The catalysts were thoroughly characterized with respect to surface area using BET (Papers I, III), Ag particle distribution using UV-Vis (Paper I) and oxidation state using XPS (Paper I, II). The catalytic activity has mainly been evaluated on monolith samples in synthetic gas flow reactors (Papers I-V), however powder micro reactor was also used in Paper IV. The surface reactions have also been studied using DRIFTS (Paper III). In addition to the lab-scale experiments, the most promising catalyst was up-scaled and evaluated in an engine bench setup, using a one-cylinder engine as the exhaust gas generator (Paper V).

4.1. Catalyst preparation

Catalyst powder synthesis

The Ag/Al_2O_3 samples were prepared by a sol-gel method including freeze drying [50]. A sol is defined as a solid suspension, where the size of the dispersed solid is so small that it prevents the particles from sedimentation by Brownian motion. The prepared samples had a nominal silver loading of 2, 4 and 6 wt. %, respectively (Paper I-V). In addition to the pure Ag-alumina, the corresponding samples were prepared with addition of 100 and 500 ppm platinum. The catalysts are denoted as: Ag(silver loading in %)Pt(platinum doping in ppm) (Paper I-II, IV-V), *e.g.* Ag2Pt100 contains 2 wt. % Ag and 100 ppm Pt. The alumina precursor (aluminum isopropoxide, >98%, Aldrich) was added to milli-Q water and heated to 82°C during vigorous stirring. Subsequently, the silver precursor ($AgNO_3$, >99%, Sigma), and for the doped samples a platinum precursor ($Pt(NO_3)_2$, solution type K, Heraeus), was added. The pH was adjusted to 4.5 by addition of HNO_3 (10%, Fluka), resulting in the formation of a sol. The sol was stirred for 12 h, after which a major part of the solvent was removed using a heated vacuum system.

When micro-porous materials are thermally dried, localized boiling may occur resulting in considerable pressure variations in the micro-pours channels. This may cause pores to collapse, which will reduce the surface area of the material. In addition, finely dispersed atoms/clusters may, due to the high temperature, migrate to the edge of the pores and agglomerate to larger particles. In order to preserve the micro-porous structure of the γ-alumina, the gel can instead be dried using a freeze-drying method, where the solvent is removed via sublimation. This prevents both pore collapse and active phase migration. The samples were initially frozen using liquid nitrogen. The frozen samples were then subjected to pressures below 5 hPa and -110°C in a Freeze dryer (SCANVAC, CoolSafe 110-4 Pro) resulting in a cryogel.

The freeze-dried gel, *i.e.* cryogel, consisting of aluminumoxyhydroxide, is subsequently heated to 600°C in air where it phase transforms to γ-alumina. The sample is placed in an oven and the temperature is raised at 2°C/min from RT to 600°C. In addition to the solid state reaction, the sample is also purged from undesired compounds from the synthesis, such as remaining nitrates and carbon containing species.

Monolith coating

The majority of the activity measurements were performed on catalyst powders, which were deposited on monoliths. For the standard Synthetic gas bench experiments (SGB) (Paper I-V), the monoliths were 20 mm in diameter and 20 mm in length. For the experiments performed in the pilot-scale reactor (PSR) (Paper V), the monoliths required had a diameter of 85 mm and a length of 90 mm.

A wash-coat slurry was prepared with 20 wt. % (bench-scale) or 15 wt. % (pilot-scale) dry content, where the dry part consisted of 20 wt. % AlOOH-binder (Disperal P2, Sasol) and 80 wt. % catalyst powder. The solvent consisted of 50 wt. % H_2O and 50 wt. % ethanol for the bench-scale monoliths, and 67 wt. % H_2O and 33 wt. % ethanol for the pilot-scale monoliths. Additional solvent and HNO_3 were added in order to control the viscosity and pressurized air was used to remove excess slurry in the monolith channels. The monoliths were submerged in the slurry, dried at 90 °C and then subjected to a fast calcination at 600 °C in air for 2 to 5 min. The wash-coating procedure was repeated until sufficient amount of wash-coat (20 wt. % of the final weight) had been deposited, where after the coated monolith samples were calcined in air (600 °C, 3 h). The pilot-scale monoliths were subsequently canned prior to their installation in the PSR.

4.2. Catalyst characterization

4.2.1. Surface area measurements

The total surface area of a catalyst can be determined according to the BET-theory [80], which is based on physical adsorption of gas molecules on a solid surface. The theory assumes that gases adsorb on a solid surface in infinite mono-layers and that there is no interaction between these adsorption layers. The Langmuir isotherm, which relates the coverage of the adsorbate on a solid surface to gas pressure or concentration of a medium above the solid surface at a fixed temperature, is applied and extended to function for several layers. In practice, physisorption of nitrogen at the condensation temperature of N_2, i.e. 77 K, is used and by performing measurements at different equilibrium pressures, a linear plot can be derived (adsorbed amount vs. pressure). From the slope and the intercept of this plot, using the known projected area of the nitrogen molecule, calculations using the ideal gas law and Avogadro's constant result in the specific surface area of the investigated material [81]. The measurements in this work were performed using a Micrometrics Tristar 3000 instrument with nitrogen sorption at 77 K (Paper I, II). The samples were dried in vacuum at 225°C for 2 hours before the measurements. The specific surface areas showed a high consistency for all samples with a high surface area in the range 192 ± 23 m^2/g.

4.2.2. X-ray photoelectron spectroscopy

One important aspect of the catalyst surface properties is the oxidation state of the active species, which can be measured using X-ray photoelectron spectroscopy (XPS). XPS utilizes a highly monochromatic x-ray beam, which irradiates the sample and uses the photoelectric effect [1, 82]. The x-rays are absorbed and photoelectrons are emitted. The kinetic energy of the emitted electrons is equal to the difference between the energy of the x-rays and the binding energy of the emitted electrons [82]. The intensity of the emitted photoelectrons is measured as a function of the kinetic energy [1] and by varying the energy of the monochromatic incoming x-rays, a spectra of the binding

energies is derived. The sample is initially studied with a fast sweep, locating the existing peaks, where after the peaks are studied with eight sweeps at high resolution. As the sample is radiated some charging of the sample may arise. To compensate for this potential charging, all spectra are calibrated with respect to the carbon C 1s peak at 284.5 eV [83]. The experiments in this work (Paper II) were performed using a Perkin-Elmer PHI 5000 C instrument, with a monochromatic Al K_α source.

4.2.3. UV-vis spectroscopy

The UV-vis spectroscopy gives information about the electronic structure from the absorption bands between ultraviolet and visible light [84]. The size of the silver species, *e.g.* silver ions or metallic silver, correlates to an absorption band, hence by analyzing the absorption spectra, the different silver species present can be determined. The information relates to the electronic levels in the atoms, ions, complexes or molecules. When studying solid catalysts, as is the case in this work, the diffuse reflectance from the powder sample is analyzed. This radiation derives from the incoming radiation, which is absorbed and then reflected after multiple scattering. The frequency of the reflected beam relates to the transition energy between different orbitals in the atom.

In this work, the fresh and aged 2 and 6 wt. % Ag-alumina samples, pure or doped with 500 ppm Pt (Paper I) were studied using a Varian Cary 5000 UV-vis-NIR spectrophotometer, with Labsphere Spectralon reference.

4.3. Catalyst performance

4.3.1. Gaseous compound measurements

During this work, many techniques have been used in order to determine the composition of inlet and outlet gases. This chapter describes the techniques used in the different reactor setups, described below. The main instrument for gaseous species concentration determination has been a Fourier transformed infrared (FTIR) gas analyzer. In addition, due to detection limits for non-polar species in the FTIR a chemiluminescence (NO_x analyzer) instrument were used.

The outlet gas concentrations in Paper I-III and V were measured using a FTIR gas analyzer (MKS instruments, MultiGas 2030 HS). Fourier transformed infrared spectroscopy is a vibrational spectroscopy which utilizes the infrared region of the electromagnetic spectra [84]. As a sample is subjected to infrared radiation it induces vibrations in the molecular bonds, provided the dipole moment of the molecule changes during the radiation. The vibrations are caused by an overlap between the IR- frequency and the frequency of the molecular bond, especially in the middle region (4000-200 cm^{-1}), which corresponds to the energy of vibration [84]. A molecule does not have to be a permanent dipole to be IR-active if a dipole is induced by the radiation, however symmetrical molecules such as O_2 and N_2, cannot be detected with FTIR [85]. The vibrations correspond to absorption peaks with specific frequencies. A specific molecule bond will have an absorption peak within a certain frequency range depending on its close surrounding. The quantitative concentration of the bond can be determined by measuring the area of the absorption peak [84]. The absorption spectrum is unique for a specific compound, hence both qualitative and quantitative analysis of a compound is possible, however many species have partially overlapping spectra. This may result in difficulties when distinguishing between different compounds, hence it is beneficial to have some knowledge about the samples in advance.

The advantage of using FTIR, as compared to conventional infrared spectroscopy, is that FTIR has an interferometer, making it possible to measure all the frequencies in the infrared region simultaneously, resulting in extremely fast measurements. The IR-beam is first sent through a beam splitter, where after one part of the beam is reflected on a stationary mirror and subsequently sent through the sample to the detector. The other part of the beam is reflected in a movable mirror and then sent back through the sample to the detector, resulting in a difference in the length the light has to travel, controlled by the position of the movable mirror. The positive/destructive interference data from the interferometer is a graph of output light intensity versus retardation, retardation being the difference in path-length for the light hitting the movable mirror and the stationary mirror [86], respectively.

As stated previously, the FTIR analyzing technique cannot detect molecules which cannot induce a dipole momentum. In order to monitor symmetric molecules, *e.g.* H_2, N_2 and O_2, a mass spectrometer can be employed. Although very efficient for many species, as the specific mass of the ions are detected, overlapping signals may occur, *e.g.* CO and N_2. The technique uses an ionization chamber where the compounds are charged and then separated by their mass-to-charge ratio (m/z) [87]. The ions are subsequently collected and the number of ions per mass is translated to a mass spectrum. The ion detector can be constructed in different ways. The main principle is however that the ion beam is subjected to an electric field, which will bend the beam. For the single focusing magnetic mass analyzer, the beam is collected in a curved trajectory. The m/z will determine the radii of the curvature as a function of the field strength and voltage with which the ions are accelerated. By alternating the accelerating voltage and the field strength, the m/z, *i.e.* the species, can be detected. Mass spectrometry was used to analyze the effluent gases for the DRIFTS experiments in Paper III.

In Paper IV, the NO_x reduction was also measured using a NO_x analyzer, which utilize chemiluminescence in detecting the NO and NO_2 concentrations. The technique is based on the emission of light as a result of a chemical reaction. NO reacts with ozone and a luminescent active NO_2* molecule is formed. As the NO_2 molecule relaxes, it will emit one photon for every NO molecule that originally reacted, which can be amplified though photomultipliers. In the case of gas composed of a mixture of NO and NO_2 the gas is first analyzed for NO, via the $NO + O_3 \rightarrow NO_2^* + O_2$ reaction, where after all the NO_2 in the feed is converted to NO and then run though a second NO_x analyzer. By subtracting the NO signal, determined by the first analyzer, from the total NO_x signal, the NO_2 concentration can be determined.

4.3.2. Synthetic gas flow reactors

The catalytic performance for lean NO_x reduction was evaluated, both at steady-state (Paper I-II, IV-V) and ramped temperature (Paper III-IV) conditions, in a continuous synthetic gas bench (SGB) reactor, Figure 3. The SGB was also used for mild ageing of the catalytic samples in Paper II. In papers I-V the monoliths were wash-coated onto cordierite monoliths and in Paper IV the catalysts were also investigated in powder form. The reactor chamber for the monolith experiments consisted of a horizontally mounted quarts tube (L=80 cm, ID=22 mm), which was heated by a metal coil (PID regulated, Eurotherm) and insulated with quartz-wool (Paper I-III, V). The synthetic gas flow reactor in Paper IV consisted of a quartz tube encased in a tube furnace (Lindberg Blue/M) [88]. The monolith was wrapped with thermally cleaned fiberglass strands and placed at the outlet of the reactor chamber. Three type K thermocouples were placed inside the reactor chamber close to the

monolith; 5 mm upstream, 5 mm downstream, and at the midpoint of the monolith, to monitor catalyst temperatures. The quartz tube was filled with 3 mm quarts beads upstream of the monolith, ensuring a uniform temperature profile of the gases. The monolith sample was placed close to the outlet, maximizing the gas heating, with uncoated monoliths before and after to minimize heat-losses from radiation, as described by Kannisto *et al.* [50]. The powder reactor was equipped with U-shaped quartz tubes (ID = 6 mm) inside a furnace. The catalytic powder (100 mg) was kept in place by two small quartz wool plugs placed just over a burr in the quartz reactor tube and on top of the catalytic powder [89, 90]. The temperature was measured using a type K thermocouple, placed in the center of the catalyst bed, and controlled by PID-controllers (Eurotherm). The inlet gas composition was controlled by separate mass flow controllers (Bronkhorst Hi-tech, Paper I-III, V; MKS Instruments, Paper IV) and the outlet gas composition in Paper I-V was analyzed using a FTIR gas-analyzer (MKS 2030 HS). In addition, two NO_x analyzers were used in Paper IV. Water (corresponding to 5%) and liquid hydrocarbon (n-octane or NExBTL), used in Paper I-III, V, were introduced separately to the reactor chamber via controlled evaporator mixer systems (CEM, Bronkhorst Hi-Tech). The system is composed of a liquid mass flow controller and a gas mass flow controller for carrier gas, connected to a small furnace where the HC is vaporized and subsequently feed to the reactor via heated tubes. In Paper IV water was introduced using a custom vapor delivery system consisting of a HPLC pump (Eldex Laboratories), which introduced the liquid to a 200 °C inert gas feed via a stainless steel capillary. The capillary was wrapped around a heating cartridge, prior to being introduced to the gas. The reducing agent was introduced by a syringe pump (Chemyx) through a stainless steel capillary into a preheated inert carrier gas stream. All gas pipes up-stream the reactor was heated to approximately 200 °C in order to prevent reactions prior to the reactor, while preventing condensation. The GHSV was keep at approximately 35 000 h^{-1} for all monolith experiment and the powder experiments were performed at 50 000 h^{-1}.

The catalyst samples were pretreated in 10% oxygen and with inert balance gas at 550°C, prior to all reactor experiments. For all measurements at steady-state, the outlet concentrations were monitored ensuring that steady-state was reached. The C/N molar ratio was kept constant at 6 during all experiments. The Ag2 and Ag6 samples in Paper II were also subjected to hydrothermal treatment at 500°C in 10% O_2 and 10% H_2O, with argon balance, for 12 hours. In Paper III, the catalysts were evaluated using transient (cooling) temperature experiments, with ethane, ethene and ethyne as reducing agents. Formation of nitrogen containing species, other than NO and NO_2, *i.e.* NH_3, HNCO, N_2O and cyanide species, were monitored and the concentrations were determined to be negligible in papers I-III and V. In Paper IV, a significant concentration of NH_3 was detected when using EtOH as the reducing agent. These results therefore also contain the NH_3 yield, but the total NO_x outlet concentration *i.e.* the basis for the NO_x reducing calculations, does not contain NH_3. Instead, the NO_x reduction calculations (Papers I-V) were derived in accordance with Eq. 1 and 2.

$$NO_x = NO + NO_2 \qquad (1)$$

$$NO_x \text{ reduction } (\%) = 100*(NO_{x,in} - NO_{x,out})/ NO_{x,in} \qquad (2)$$

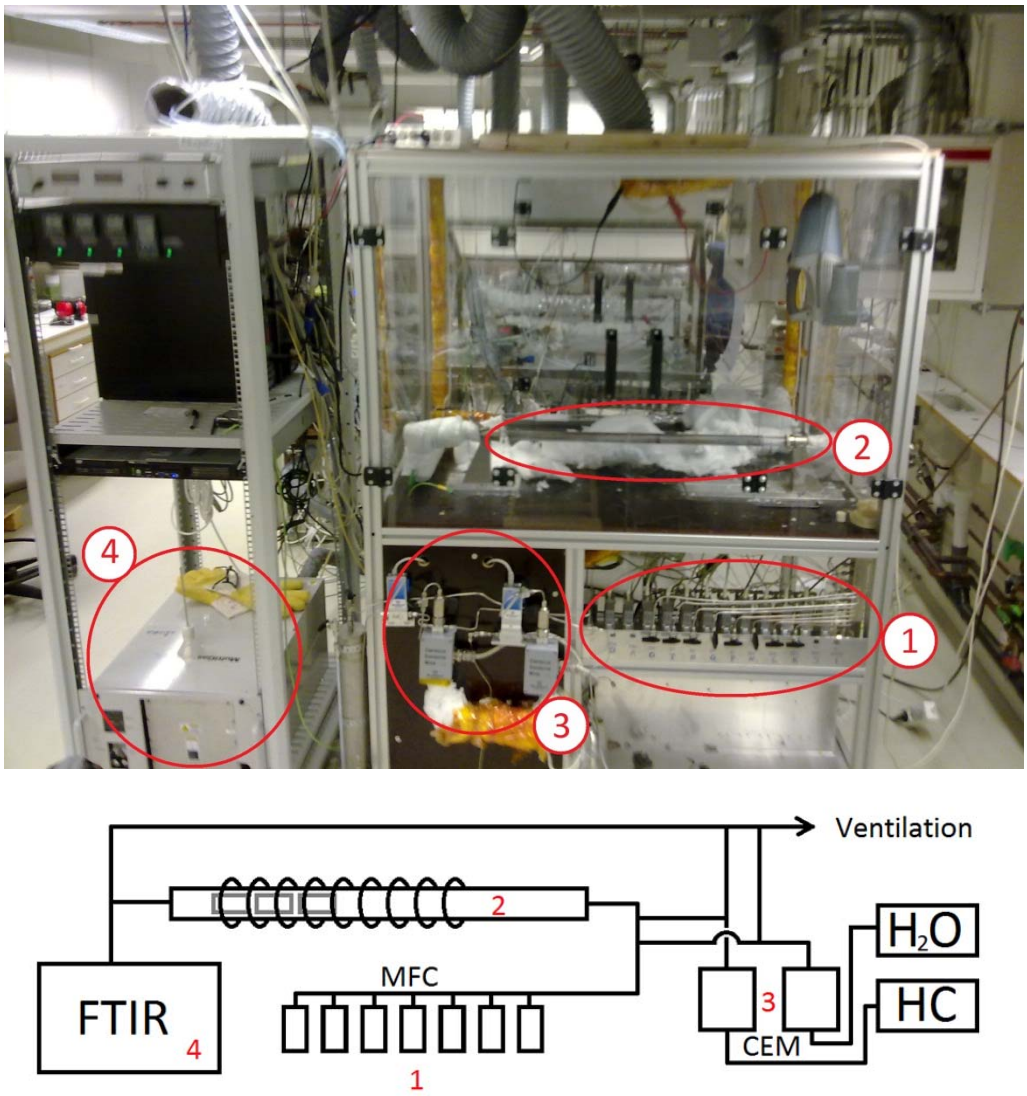

Figure 3: A synthetic gas bench reactor showing 1) MFC-system, 2) metal coil heated reactor chamber, 3) CEM-system and 4) FTIR gas analyzer.

The hydrocarbon conversion (Paper I, II, and IV) was determined according to Eq. 3 and 4.

$$C_{1,out} = CO_{out} + CO_{2,\,out} \qquad (3)$$

$$HC\ conversion\ (\%) = 100*(C_{1,\,out}/C_{1,in}) \qquad (4)$$

4.3.3. Engine bench reactor setup

The pilot-scale reactor (PSR) experiments (Paper V) were performed at Advanced Technology and Research, Department of energy efficiency and environment, Volvo Group Trucks Technology, Sweden. In the PSR experiments the HC-SCR catalyst ($Ag4Pt100/Al_2O_3$) was evaluated in real exhaust gases together with hydrogen supplied from a fuel reformer, and from a gas bottle, and NExBTL was used as reducing agent as well as fuel in the fuel reformer.

The exhaust gases were generated by a genset (DX 6000 TE XL C, Yanmar) propelled by VSD10 diesel. The genset generated an exhaust gas flow of ~450 dm^3/min containing ~420 ppm NO_x, depending on the operation mode. The exhaust gases were initially led through a diesel oxidation catalyst (DOC) (l = 150 mm, Ø = 140 mm) with a separate diesel injection. The DOC was used to regulate the heat of the exhaust gases and the operating temperature for the HC-SCR catalyst. The exhaust gas then passed through a diesel particulate filter (DPF), removing the particulates, and subsequently to the Ag/Al_2O_3 HC-SCR catalyst. The Ag/Al_2O_3 catalyst consisted of two sequential monoliths (l = 95 mm, Ø = 90 mm, V_{tot} = 1.2 dm^3), resulting in an approximate GHSV of 22,300 h^{-1}. Prior to the HC-SCR catalyst an air-assisted diesel injection system and a hydrogen injection nozzle were mounted. The hydrogen could be fed either from a gas bottle or from the fuel reformer. The gas composition was measured with an FTIR gas analyzer equipped with a sampling pump (MKS^{TM} 2030 *HS*). The gas composition could be monitored either upstream or downstream of the HC-SCR catalyst. The temperature of the exhaust gases was measured before the HC-SCR catalyst. An overview of the system used in the PSR experiments can be seen in Fig. 2. The physical and chemical properties of the fuels used during the experiments are given in Table 1.

The fuel reformer consisted of a vertically mounted stainless steel reactor with external heating. To avoid bypassing around the monolith, it was wrapped in ceramic tape prior to mounting it in the reactor. The size of the monolith was 9.4 cm^3 (l = 30 mm, Ø = 20 mm). The gases (N_2 and synthetic air) and fuel were regulated by three separate mass flow controllers (MFC) (Brooks Instruments). The water was pumped with a continuous syringe pump. The water and fuel was introduced and vaporized prior to the reactor. In front of the monolith a quartz plate was mounted to enhance the mixing of the reactants and ensure complete evaporation of the liquid reactants. The reformate could either be used as hydrogen source for the HC-SCR or be analyzed by an IR gas-analyzer (Sick Maihak). The concentrations of CO, CO_2, CH_4, O_2 and H_2 were analyzed based on dry reformate. The GHSV was approximately 20,000 h^{-1}, H_2O/C = 3.8 and O_2/C = 0.4. The fuel reformer was operating at two different operating points, depending on the H_2 concentration (~1200 ppm or ~2000 ppm H_2) in the exhaust gas feed. The volumetric flow of reformate produced at the two operating points were 3.2 dm^3/min and 3.9 dm^3/min, and the temperatures were 800 and 850 °C, respectively. The H_2O/C ratio used in the PSR setup was higher, *cf.* the SGB setup, to enable a higher cleaning rate of the catalyst surface, since the catalyst could potentially be exposed to diesel in liquid state due to limitations in the diesel injection system.

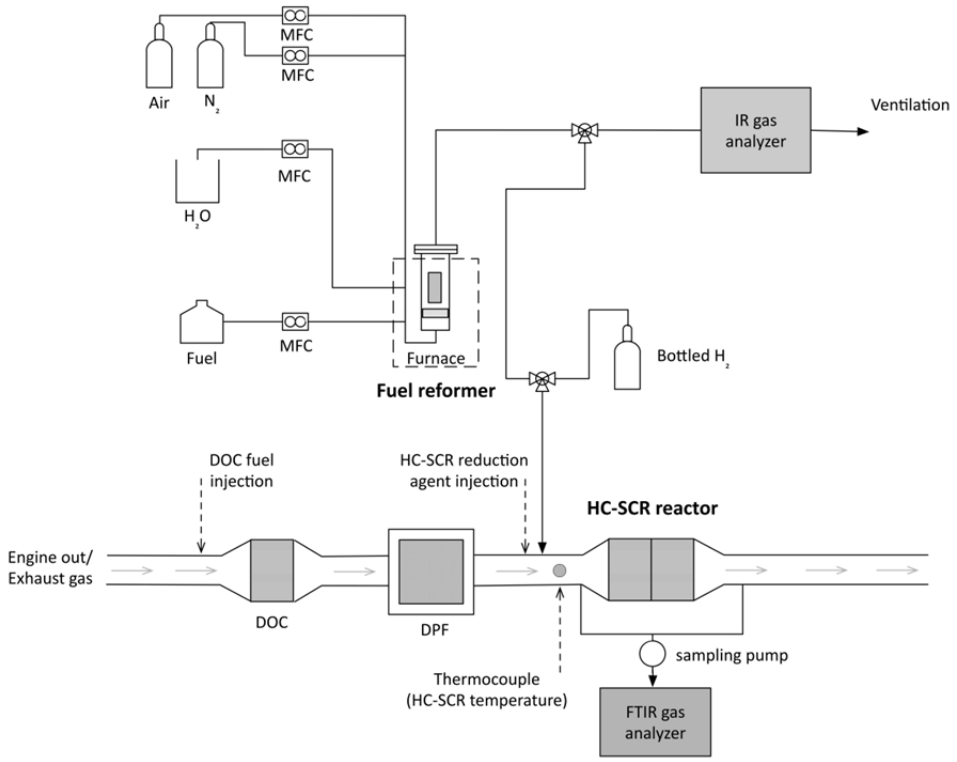

Figure 4: Schematic sketch of the pilot-scale setup used for evaluating the HC-SCR catalyst together with real exhaust gases produced from a genset engine. The hydrogen could either be introduced from the separate fuel reformer or directly from a gas bottle. The fuel used in the fuel reformer as well as reducing agent was the commercial biodiesel, NExBTL. The gas and liquid flows to the fuel reformer were controlled by mass flow controllers (MFC). Prior to the HC-SCR catalyst, a diesel particulate filter (DPF) was mounted to remove the particulates from the engine. To enable heating of the exhaust gases, a diesel oxidation catalyst (DOC) with separate HC dosing was used.

4.3.4. DRIFTS reactor setup

The Diffuse Reflectance Infrared Fourier Transform Spectroscopy (DRIFTS) system utilizes the same technique as FTIR, described in 4.3.1, however the system is constructed to investigate the adsorbed species on the catalytic sample surface *cf.* gas in FTIR (Paper III).

The flow though DRIFTS reactor experiments in Paper III were performed using a Bio-Rad FTS6000 spectrometer equipped with a high temperature reaction cell (Harrick Scientific, Praying Mantis™) [9, 91]. The gas composition, introduced to the DRIFT cell, was controlled using separate mass flow controllers (Bronkhorst Hi-Tech, low ΔP), and the outlet gas composition was monitored continuously by a quadrupole mass spectrometer (Balzers QMS 200) via a quartz capillary. The sample was pretreated with 10% oxygen at 500 °C for 30 min and then pure Ar at 450 °C for 20 min at a total flow rate of 100 mL/min. Background spectra (60 scans at a resolution of 1 cm^{-1}) were collected for fresh samples under Ar atmosphere. Step-response experiments were subsequently performed at 450 °C, where the hydrocarbon (C_2H_4 and C_2H_2) and NO supply was switched on and off. IR spectra with 1 cm^{-1} spectral resolution were collected with an acquisition frequency of 0.1 Hz.

5. Results and discussion

This thesis aim to cover a wide scope, ranging from the active sites and stability of the Ag/Al_2O_3 system, to effects of, and challenges from, up-scaled catalytic samples evaluated at real engine conditions. The results will be discussed in the following fashion; the first section (5.1) relates to the active sites of the catalyst. The section covers characterization of the samples, thermal stability and the effect of platinum doping (Paper I-II, IV). The second section (5.2) describes the influence of different reducing agents, ranging from model hydrocarbons (n-octane, C_2H_x) to real hydrocarbon fuels (NExBTL, EtOH) and how the platinum doping influences these aspects (Paper I-V). The last section (5.3) describes the process of up-scaling, with real exhaust effects, and the benefits and challenges which relates to such experiments (Paper V).

5.1. Influence of the active phase

The Ag-alumina catalysts were investigated using both UV-vis spectroscopy (Paper I) as well as X-ray photoelectron spectroscopy (XPS) (Paper I, II) in order to retrieve information about the nature and distribution of the silver species. The state of silver is thought to be of crucial importance in regards to the activity for NO_x reduction [52]. XRD was also used, however due to the amorphous nature of the alumina, and the small Ag cluster/particle sizes, this method was deemed redundant. Previous UV-vis studies on Ag/Al_2O_3 suggest that ionic silver species (Ag^+) show absorption peaks in the range between 190 and 230 nm [92, 93]. Peaks at 290-350 nm are ascribed to small silver clusters ($Ag_n^{\delta+}$), and peaks over 390 nm are suggested to derive from metallic silver (Ag^0) [92, 93]. The UV-vis studies were performed on both fresh and aged pure Ag-alumina samples, as well as on Ag-alumina catalysts doped with 500 ppm of platinum. Sol-gel synthesized pure γ-alumina was used as a reference and this spectrum was subtracted from the Ag-alumina data, resulting in a graph displaying the silver absorption intensity only. The adsorption bands of different silver species have been studied intensely, and the absorption spectra were deconvoluted as follows: silver ions (Ag^+) P1=230 nm [92], silver clusters ($Ag_n^{\delta+}$) P2=300 nm and P3=360 nm [92], and metallic silver (Ag^0), ascribed to peaks above 390 nm, was determined by best fit to 425 nm and 545 nm. The absorption spectrum for Ag6, in Paper II, with deconvolution peaks as well as the sum of the peaks, are shown in Figure 5. The area of the specific peaks in relation to the total absorption gives the relative amount of the different silver species. The results, shown in Table 1, indicate that the relative amount of Ag^+, $Ag_n^{\delta+}$ and Ag^0 species remains very similar in response to both alteration of the silver loading and to Pt doping (Paper I). The overall UV-vis absorption increases for the samples in the order Ag2 < Ag2Pt500 < Ag6 < Ag6Pt500. The peaks around 230 nm and 360 nm are clearly visible for all samples and the peak at 300 nm is visible for the 2 wt. % Ag samples.

The UV-vis data indicate that the ratio of ionic silver species, small silver clusters and metallic silver particles are similar for the Ag2, AgPt500, Ag6 and Ag6Pt500 samples (Paper I). However, a slight increase of the ionic species, at the expense of the metallic ones, is observed as the silver loading is increased (Table 1). Platinum doping appears to alter the ratios slightly for the 2 wt. % Ag sample, with a small increase of observable ionic species, but no change in the relative ratio is seen upon doping of the Ag6 sample. This may be related to the abundance of silver for this sample, rendering the effect of platinum negligible. Furthermore, no additional UV-vis peaks characteristic for platinum are observed for the Pt-doped samples, most likely due to the low amounts of Pt doping. However, as the levels of platinum are very low, absorption peaks for Pt is thought to be hard to

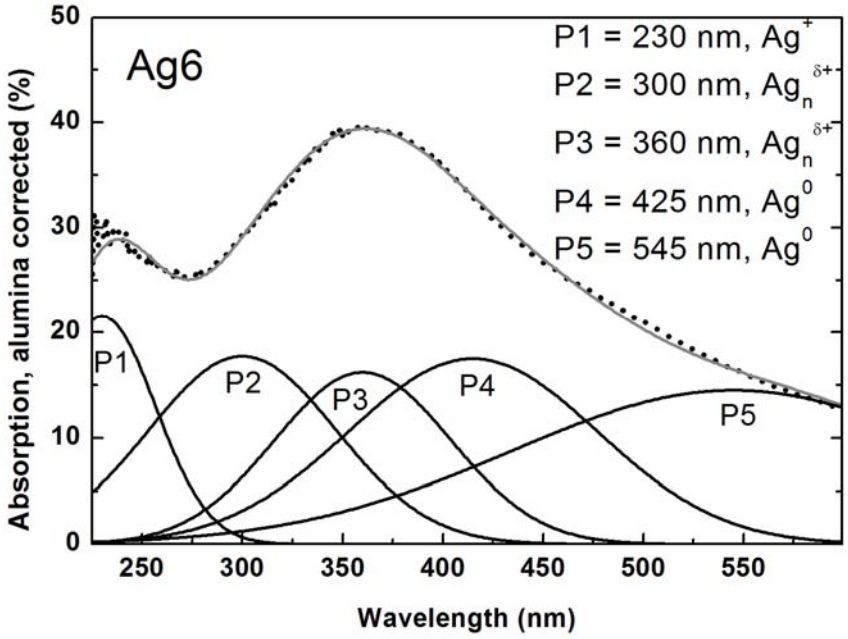

Figure 5: UV-vis spectrum (with alumina spectra subtracted) for Ag6 with total absorption (dotted line), deconvolution peaks (P1-P5) and the sum of the deconvolution peaks (solid line).

detect. The overall UV-vis results indicate that no significant differences in relative ratio of silver species can be seen for the four samples.

In addition to UV-vis spectroscopy, the samples were investigated using XPS. The binding energy for the Ag $3d_{5/2}$ peak as well as the distance between the Ag $3d_{5/2}$ and the Ag $3d_{3/2}$ peaks, for the above mentioned Ag2, Ag2Pt500, Ag6 and Ag6Pt500 samples (Paper I), as well as for the fresh and aged 2 and 6 wt. % samples (Paper II), are shown in Table 2. The results from pure and Pt doped samples show that the $Ag3d_{5/2}$ peak is centralized around 367.7 eV, similar to results by Bukhtiyarov *et al.*, validating the existence of Ag^+ species [94], with a peak to peak distance between 5.9 and 6.2, in accordance with literature data [95]. The results further indicate that the ratio between different silver species does not change with silver loading and/or Pt-doping.

Table 1: Sample denotation, specific surface area (BET) and relative amount of Ag^+, $Ag_n^{\delta+}$ and Ag^0 (UV-vis) of the Ag/Al_2O_3 samples.

Sample composition	**Sample designation**	**SSA[a] (m^2/g)**	**$Ag^{+,b}$ (%)**	**$Ag_n^{\delta+,c}$ (%)**	**$Ag^{0,d}$ (%)**
2 wt. % Ag/Al_2O_3	Ag2	189	11	38	51
2 wt. % Ag/Al_2O_3 w. 500 ppm Pt	Ag2Pt500	215	14	39	47
6 wt. % Ag/Al_2O_3	Ag6	167	17	37	46
6 wt. % Ag/Al_2O_3 w. 500 ppm Pt	Ag6Pt500	182	17	37	46

[a] BET surface area. [b] Ag^+ ionic silver, P1 at 230 nm [92]. [c] $Ag_n^{\delta+}$ silver clusters P2=300 nm and P3=360 nm [92]. [d] Ag^0 metallic silver P4=415 nm and P5=545 nm.

Table 2: Binding energy for the $Ag3d_{5/2}$ peak and the distance between the $Ag3d_{5/2}$ and the $Ag3d_{3/2}$ peaks for fresh and aged 2 and 6 wt. % Ag/Al_2O_3 samples (Paper II) as well as 2 wt% Ag/Al_2O_3, with 0 and 500 ppm platinum, 6 wt. % Ag/Al_2O_3, with 0 and 500 ppm platinum (Paper I).

	Ag2 fresh	**Ag2 aged**	**Ag6 fresh**	**Ag6 aged**	**Ag2Pt500 fresh**	**Ag2Pt500 aged**	**Ag6Pt500 fresh**	**Ag6Pt500 aged**
BE (eV)	367.5	367.9	367.9	367.9	367.6	367.7	367.7	367.7
ΔBE (eV)	6.1	6.1	6.1	6.2	5.9	5.9	6.0	5.9

As catalyst durability is a key property in exhaust after treatment, the influence of hydrothermal aging was investigated (Paper II). The samples were hydrothermally (HT) treated at 500°C in the presence of 10% H_2O and 10% O_2 with argon balance for 12 hours in order to study the initial deactivation. The Ag2 and Ag6 samples were investigated in order to evaluate the influence of Ag-loading on the lean NO_x reduction performance for fresh and aged catalysts, using n-octane as reducing agent. The influence of varying the reducing agent was also investigated and is further discussed in section 5.2. In general, the hydrothermal treatment results in a slight increase in the lean NO_x reduction activity for the samples. Furthermore, a higher silver loading results in an increased activity for NO_x reduction. Whilst the fresh 2 wt. % Ag sample exhibit somewhat higher NO_x reduction at temperatures between 225 and 325°C, as compared to the HT-treated sample, the activity of the Ag6 sample appears to be relatively unaffected by the HT-treatment in this

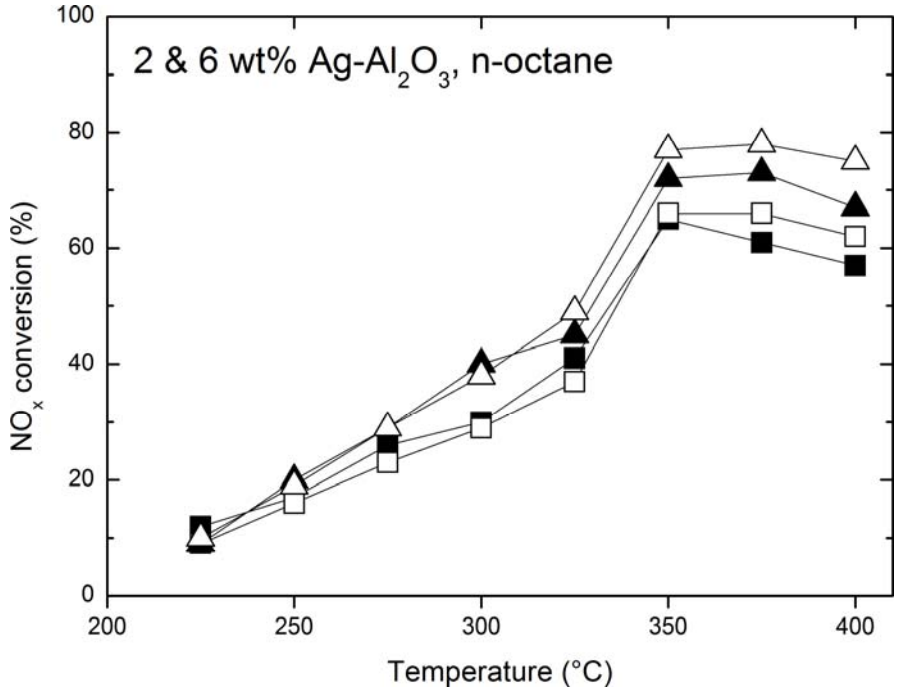

Figure 6: NO_x reduction from flow reactor experiments for fresh (closed markers) and hydrothermally treated (open markers) 2 (■, □) and 6 wt. % (●, ○) Ag/Al_2O_3 using n-octane as reducing agent. Inlet gas composition: 200 ppm NO, 10 % O_2, 1000 ppm H_2, 5 % H_2O and Ar_{bal}, C/N=6. GHSV = 33, 200 h^{-1}.

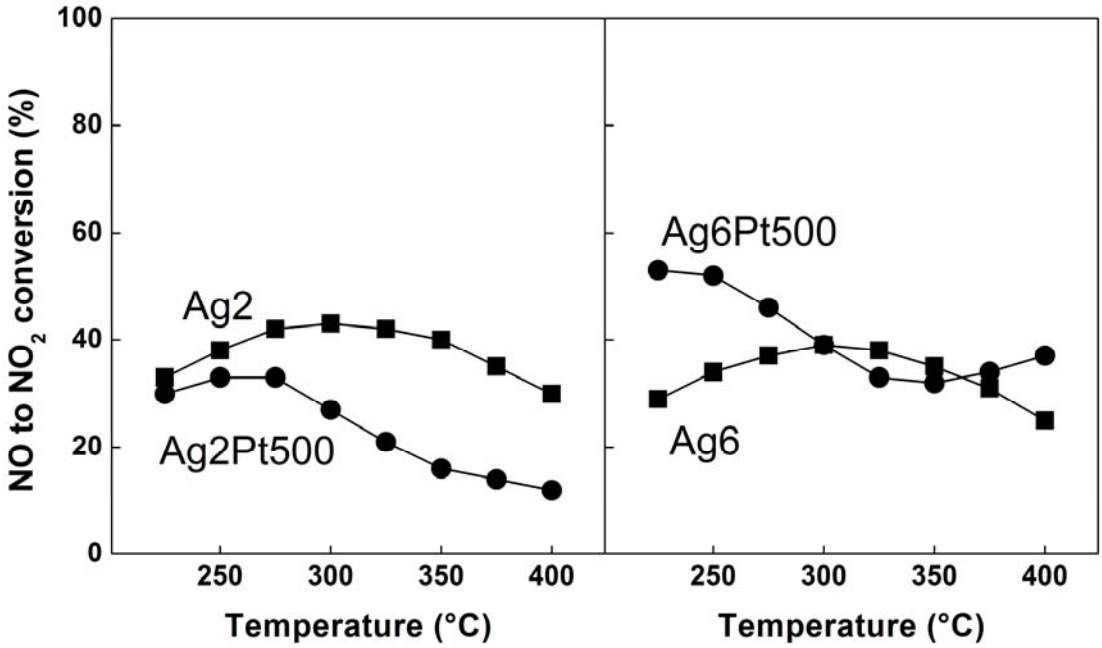

Figure 7: The NO to NO_2 conversion from NO oxidation experiments in excess oxygen is illustrated for 2 wt. % Ag/Al_2O_3 with 0 or 500 ppm platinum (left panel) and for 6 wt. % Ag/Al_2O_3 with 0 or 500 ppm platinum (right panel). Inlet gases: 200 ppm NO, 10% O_2, 1000 ppm H_2, 5% H_2O, Ar_{bal}. GHSV = 33,200 h^{-1}.

temperature interval. Above 350°C, HT-treatment results in a slight increase in the NO_x reduction over both catalysts, reaching a maximum of 66% at 350°C for the Ag2 sample and a maximum of 78% at 375°C for the Ag6 sample (Figure 6). This indicates that aging at these conditions does not influence the nature of the silver to any significant degree. The effect of ageing at higher temperatures was also investigated (Paper II). It can be seen that ageing at temperatures up to 650°C is beneficial for the NO_x reduction activity of the samples, with an increase in reduction of up to 15%. However, when the ageing temperature exceeds 650°C the activity decreases severely. Furthermore, the maximum activity is located around 350°C for both the fresh samples and the samples aged between 500 and 650°C. However, when aging is carried out at temperatures of 700°C and above, this maximum shifts towards higher temperatures.

Doping Ag/Al_2O_3 catalysts with trace amounts of platinum proved to be beneficial for the low temperature NO_x reduction activity of the catalysts (Paper I, IV, V). A series of 2, 4 and 6 wt. % silver alumina samples, pure and doped with 100 or 500 ppm of platinum, were evaluated in order to further understand the effect of the Pt-doping. The effect of platinum doping on the NO_x reduction ability can be seen in Figure 8. The activity for NO_x reduction for the samples without Pt doping follow a typical volcano shape, with an increase in activity observed as the temperature is increased up to around 350°C. Above 350°C, the competing combustion reaction becomes dominant, consuming the reductant, and the NO_x reduction decreases. The Ag2 and Ag4 samples show similar performance for NO_x reduction up to 325°C. At higher temperatures however, the Ag2 sample show higher NO_x reduction. The Ag6 sample show slightly lower NO_x reduction below 325°C, compared with the Ag2 and Ag4 samples, but displays the highest NO_x reduction above 350°C.

Introducing Pt to the samples generally improves the low-temperature activity for lean NO_x reduction. However, although the activity for NO_x reduction over the Ag2Pt100 sample resembles that of the pure Ag/Al_2O_3 samples, increasing the silver loading to 4 and 6 wt. % Ag results in decreased activity for NO_x reduction at high temperatures. The Pt doped 4 and 6 wt. % Ag samples also display local minimum in NO_x reduction around 325°C, also visible for the Ag2Pt500 sample. The NO_x reduction for these samples increases again as the temperature reaches 350°C, although the activity does not reach that of the pure Ag/Al_2O_3 samples. The Ag2Pt100 sample shows the highest activity for NO_x reduction above 350°C. The results from the samples doped with 500 ppm Pt show an even higher activity at low temperatures, with the highest activity for the Ag2Pt500 sample. The decrease in activity, localized around 325°C, is observed over all Pt doped samples and becomes more prominent and starts at lower temperatures as the silver loading is increased.

To explain the dual activity regime of the Pt doped samples above and below 325°C, the effect of NO oxidation was investigated (Figure 7). The outlet concentrations of NO and NO_2 indicate that the ratio between NO and NO_2 is quite similar for the pure silver alumina samples with NO as the dominant NO_x species over the entire temperature range. For the samples doped with platinum however, the NO/NO_2 ratio is altered, showing a higher NO_2 concentration at low temperatures. At high temperatures NO is again the dominating gas phase NO_x species. For the samples with 100 ppm Pt doping, the NO and NO_2 concentrations are similar for the 2 and 4 wt. % Ag samples, whereas the NO_2 concentration is substantially higher for the 6 wt. % Ag sample. Further, for the samples doped with 500 ppm Pt, the change in NO concentration is substantial, with increasing NO concentration for increasing silver loading at higher temperatures. The NO_2 concentration follows the opposite trend with high concentrations at low temperatures, decreasing with increasing temperature. Previous studies [64] have shown that varying the inlet NO/NO_2–ratio generally have a negligible influence on the overall NO_x reduction, and that the effect of introducing NO_2 in the feed even is negative for the overall reduction of NO_x when using n-octane as reducing agent [64]. Meunier *et al.* [96] found a promotional effect when using NO_2 as reactant, however these experiments were performed with low oxygen concentrations using C_3H_8 as reducing agent. During such conditions, a strong oxidizing agent as NO_2 might be beneficial.

The overall results show that, as the catalysts are doped with platinum, the oxidation of NO to NO_2 is changed, but as stated before this is not thought to play a major role in the NO_x reduction reaction under the present reaction conditions. No clear trend from the NO oxidation experiments or the NO/NO_2 concentration during the NO_x reduction experiments is found that can explain the change in NO_x reduction activity observed for the platinum-doped samples. The change is instead believed to be related to the oxidation of the reducing agent, further discussed in 5.2.

However, the HC oxidation experiments show that the addition of platinum alters the HC oxidation properties for the Ag-alumina catalysts, resulting in two oxidation regimes. This double regime behavior, with a minimum HC conversion at 325°C, is related to the NO_x reduction activity also showing two reduction regimes. As the temperature increases, the amount of available hydrocarbons on the surface increases, possibly owing to that the inactive nitrates desorb allowing more hydrocarbons to adsorb on the surface. For the high-loaded samples with 500 ppm platinum the amount of hydrocarbon starts to poison the surface and the NO_x reduction activity starts to decrease. As the temperature reaches 325°C, the hydrocarbon oxidation over the pure silver sites

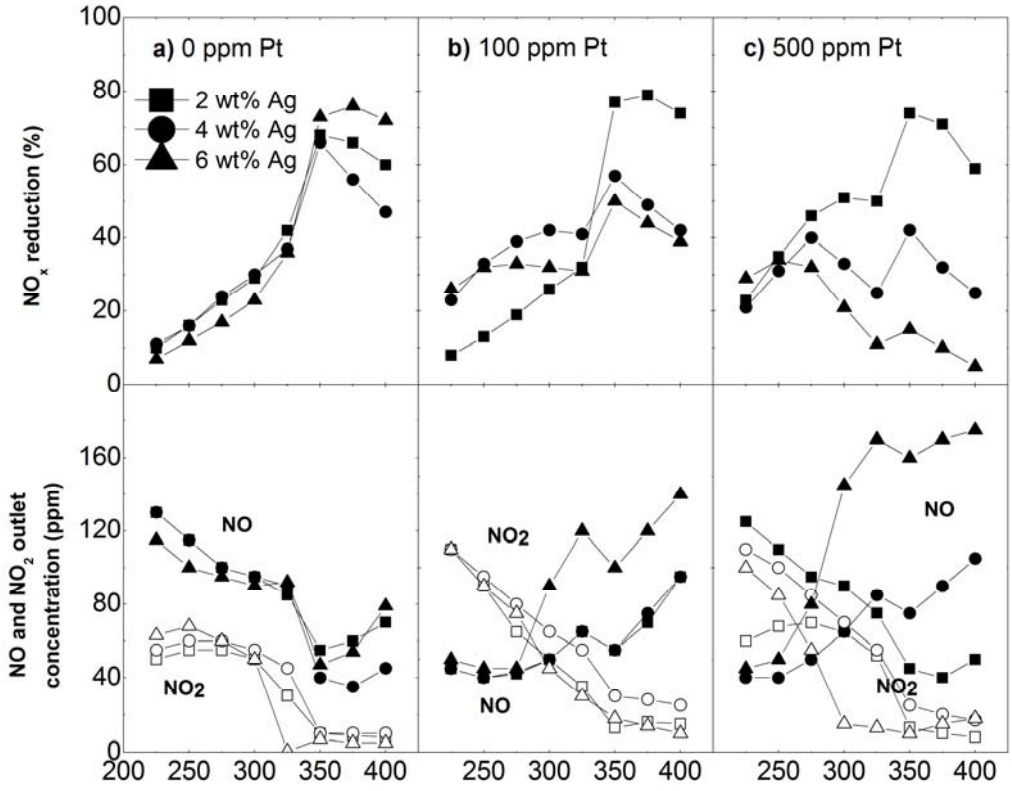

Figure 8: NO_x reduction (top) as well as outlet concentration of NO and NO_2 (bottom) from NO_x reduction experiments in flow reactor for 2 wt. % (■), 4 wt. % (●) and 6 wt. % (▲) Ag/Al_2O_3 samples without Pt (left column), with 100 ppm Pt (center column) and with 500 ppm Pt (right column). Inlet gas composition: 200 ppm NO, 10 % O_2, 1000 ppm H_2, 5 % H_2O, Ar_{bal} and n-octane as reducing agent with a C/N molar ratio of 6. GHSV = 33, 200 h^{-1}.

starts and the excess hydrocarbon is purged from the surface, resulting in a decrease in activity with a minimum around 325°C, where after the activity is recovered. Hence, the change in HC oxidation performance and the increase in hydrocarbon adsorption on the surface are suggested to be the underlying reason for the two reduction regimes for NO_x. This effect leads us to suggest that, although the NO to NO_2 formation likely is of some importance, it is the increase in sticking probability, *i.e.* hydrocarbon-surface interaction, and partial oxidation of the hydrocarbon, owing to the added platinum, that is the main factors leading to the increase in NO_x reduction at low temperatures for the Pt-doped samples. This implies that the doped samples have more available hydrocarbons on the surface, owing to higher sticking probability, and the increase in low-temperature NO_x reduction is actually a result of this effect.

The silver loading can be seen to significantly influence both the NO_x reduction activity as well as the temperature for maximum reduction, independent of reducing agent (Paper I-III). As the ratio between the surface silver species is constant for the different silver loadings (Paper II), the number of active sites probably plays a major role. A higher number of sites would decrease the distance between the different sites, likely increasing the interaction between the oxidative and reductive sites. Paper II-III also illustrates the importance of the nature of the reducing agent with emphasis on carbon-carbon bond order, hydrocarbon branching and surface sticking probability.

In concussion, the nature of the active phase is of great importance when designing an Ag/Al_2O_3 catalyst, with respect to both activity and durability. The synthesis route used in this work has been shown to result in a higher number of small silver species, particularly active for the NO_x reduction reaction. The number of small silver species is however not the only parameter of importance when designing the catalyst. The use of different types of reducing agents, discussed in the next chapter, will result in different sticking probabilities and oxidation barriers. This will hence require more or less oxidizing metallic silver sites in order to activate the reducing agent, making it accessible in the NO_x reduction reaction.

5.2. Influence of reducing agent

The fuel supply for the transport sector contains a large variety of fuels, both fossil and renewable and, as discussed in the "Biofuels" section, the supply and variety of renewable fuels will likely grow. In order to ensure a robust and reliable NO_x reduction system, the influence of different fuels on the HC-SCR process must be understood. Properties such as HC-chain length, oxygen content and over-all stability of the reducing agent can greatly affect the NO_x reduction. One key factor is likely the accessibility of the hydrocarbon, *i.e.* the amount of adsorbed surface hydrocarbons and the stability of the HC in gas phase with respect to temperature and its reactivity. The effect of different reducing agents was investigated in Paper I-V, ranging from a commercial biodiesel (NExBTL), a representative hydrocarbon for gasoline (n-octane), ethanol and ethanol/gasoline blends, and model hydrocarbons such as C_2 compounds with different bond order (C_2H_2, C_2H_4 and C_2H_6). The use of NExBTL, a biomass-to-liquid product derived from vegetable oils and animal fats consisting of n- (<10%) and iso- (>90%) paraffins [97], has been shown to result in reduced engine-out emissions of NO_x, HC and CO at heavy-duty conditions, when blended with other diesel fuels *e.g.* EN590 and EC1 *cf.* conventional diesel fuels [97].

This section will initially focus on commercial fuels and then gradually move to model hydrocarbons. The use of real fuels as reducing agents in laboratory scale does not only pose problems in a practical sense, but also results in a far more complex chemistry. The main difficulty during the experiments in this study was, however, related to practical applications. For example, environmental class 1 (MK1) diesel was initially considered as a candidate during the selection of reducing agents, however no consistent and reliable way of introducing MK1 was possible using the available equipment. This was most likely due to the aromatic content amongst other factors, hence NExBTL was chosen as the most complex reducing agent, containing no aromatic compounds, and also fulfilling the objective of using renewable fuels. NExBTL was used both during standard NO_x reduction conditions (Paper II, V) and when investigating thermal stability of the catalyst (Paper II) in order to compare a model hydrocarbon (n-octane) to real fuels. The thermal stability of the catalyst was found to be high both when using n-octane and NExBTL (Figure 9).

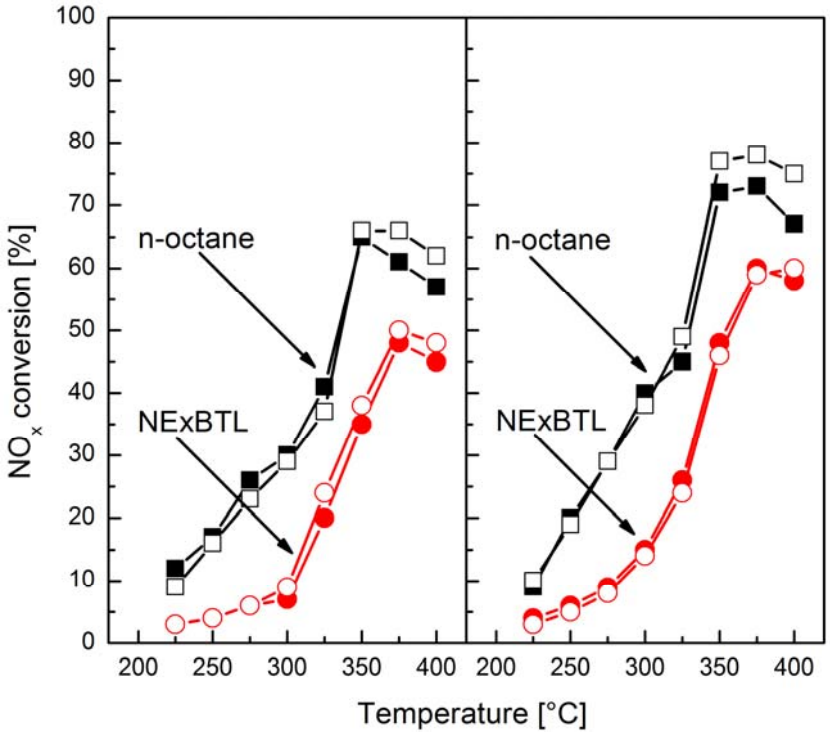

Figure 9: NO_x reduction from flow reactor experiments for fresh (closed markers) and hydrothermally treated (open markers) 2 and 6 wt. % Ag/Al_2O_3 samples using n-octane (■, □) or NExBTL (●, ○) as reducing agent. Inlet gas composition: 200 ppm NO, 10 % O_2, 1000 ppm H_2, 5 % H_2O and Ar_{bal}, C/N=6. GHSV = 33, 200 h^{-1}.

Furthermore, to investigate the effect of various types of hydrocarbons, the hydrocarbon oxidation was studied in addition to the NO_x reduction. As stated previously, NExBTL consists mainly of iso-paraffins [93] and has an approximate carbon chain-length of 16 carbon atoms compared to eight for n-octane. This difference will most likely influence the adsorption behavior of the hydrocarbons, and the high amount of branching in the NExBTL can lead to increased adsorption as compared to the n-octane. This is also supported by results from Lindfors *et al.* [98], where branched hydrocarbons display a lower activity, for both NO_x reduction and HC oxidation, compared to straight hydrocarbons. This effect was investigated over samples with different silver loadings. The 6 wt. % Ag sample does have higher number of oxidation sites than the 2 wt. % Ag sample (Paper I) and should hence be able to oxidize the adsorbed hydrocarbon to a higher degree, facilitating a slightly higher HC conversion. A sharp increase in HC conversion can be seen for all samples above 300°C (Figure 10 and Figure 11), both during the HC oxidation and the NO_x reduction experiments. This is likely owing to the reduction of Ag surface oxide species to metallic silver [99], increasing the oxidative properties and improving the HC oxidation activity. In addition, the length and branching of the hydrocarbon chain likely influences the type of oxygenated hydrocarbon species formed on the surface [98]. Hence, the surface coverage of NExBTL and/or NExBTL derived species would likely be higher in comparison with the case of n-octane, effectively poisoning the catalyst surface. This could potentially lead to a reduction of the amount of nitrogen-containing species on the surface and is thought to be the reason for the lowered NO_x reduction activity when changing from n-octane to NExBTL.

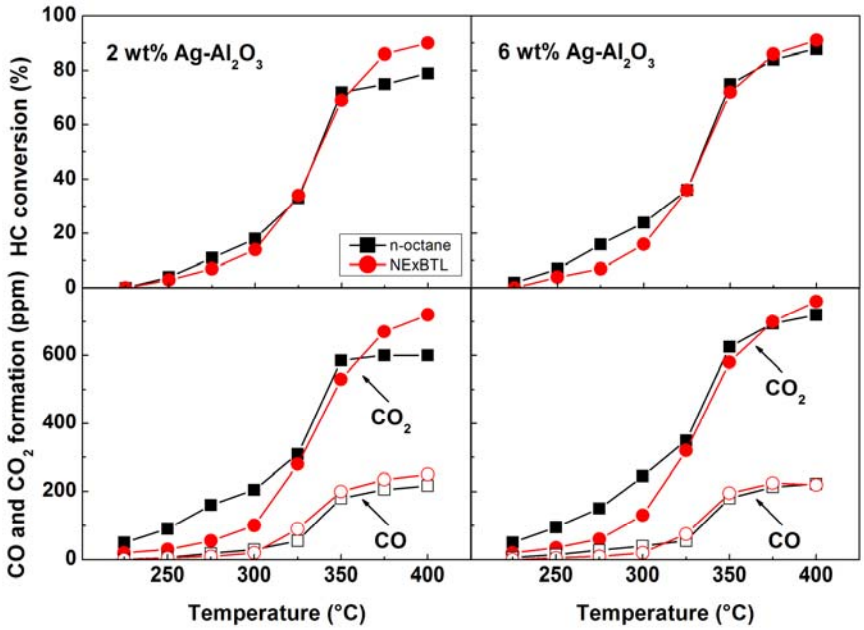

Figure 10: Hydrocarbon conversion and, CO and CO_2 formation over temperature for the Ag2 and Ag6 samples during NO_x reduction experiments, using n-octane and NExBTL as reducing agents. Inlet gas composition: 200 ppm NO, 10 % O_2, 1000 ppm H_2, 5 % H_2O, Ar_{bal} and n-octane or NExBTL as reducing agent with a C/N molar ratio of 6. GHSV = 33, 200 h^{-1}.

As stated above, the surface properties of the catalyst are of high importance when studying oxidation properties. To further understand the oxidation of the hydrocarbon over the Ag-alumina surface, separate hydrocarbon oxidation experiments using n-octane (Paper II) and hydrocarbons with different carbon−carbon bond order *i.e.* alkane, alkene, and alkyne (Paper III) were performed. Paper II also includes Ag-alumina samples doped with platinum. When comparing hydrocarbon oxidation results for the Pt-doped and pure Ag catalysts (Figure 11), the n-octane conversion for the Pt-doped samples starts at much lower temperatures. For instance, the n-octane conversion for the Ag2Pt500 sample starts already at 250°C, which should be compared to well above 300 °C for the corresponding un-doped Ag sample, similar to the steep increase in the HC-oxidation for n-octane and NExBTL during NO_x reduction experiments using pure Ag-alumina catalysts (Figure 10). The HC conversion for the Ag6Pt500 sample starts before 225°C, however the conversion increase levels out at 325°C, similar to the drop in NO_x reduction activity (Figure 8). Although the platinum decreases the onset temperature for HC oxidation, the Ag6 sample also displays a higher oxidation capacity *cf*. Ag2, seen when comparing the different C_2 compounds (Paper III). In general the hydrocarbon oxidation using C_2H_x hydrocarbons proceeds at lower temperatures and results in higher CO_2 formation over the Ag6 sample as compared to the Ag2 sample. For example, when using the C_2H_2 hydrocarbon, the Ag2 sample shows HC-conversion (seen from CO_2 formation) at 300 °C (Figure 13) whereas the Ag6 sample starts already at 250°C. This is particularly evident in the case of C_2H_4 oxidation, which starts around 350°C over the Ag6 sample but not below 450°C over the Ag2 sample. For both catalysts, the lowest activation temperature is observed for ethyne (C_2H_2) oxidation, which starts around 270 and 300 °C for the Ag6 and Ag2 samples, respectively. This is probably connected to the presence of a higher amount of metallic silver species in the Ag6 catalyst compared to the Ag2 catalyst, facilitating total oxidation in agreement with previous studies [50, 100]. Generally, the silver species most likely attain a more metallic structure as the temperature is increased (>300°C), as stated before [99],

which likely results in an adsorption/oxidation equilibrium balance, where the rate of oxidation is similar to the rate of adsorption. Hence, the surface coverage of hydrocarbons decreases and other species, *i.e.* NO_x, can adsorb and react. Moreover, the UV-vis and XPS results indicate that increasing the silver loading leads to an increase in the total number of oxidation sites (the individual Ag species ratios being constant), which results in an increase in HC oxidation at high temperature, for the high-loaded Ag samples. The increased hydrocarbon oxidation at low temperatures for the Pt-doped samples can, on the other hand, likely derive from increased adsorption energy of the hydrocarbon on the surface. Comparing the dissociation energies for different molecules on silver and platinum surfaces, the dissociation energy is always lower for platinum according to Bligaard *et al.* [77]. The authors report that the dissociative chemisorption for CH_4 on platinum cf. silver differs by 6.49 eV [77]. The Brønsted-Evans-Polansky (BEP) relation [78, 79] states that the change in activation energy follows the change in energy of the final state for the chemically dissociated molecule. Although the energy difference is likely smaller for long-chained hydrocarbons, the sticking probability, *i.e.* hydrocarbon-surface interaction, on platinum is still prone to be higher than on silver.

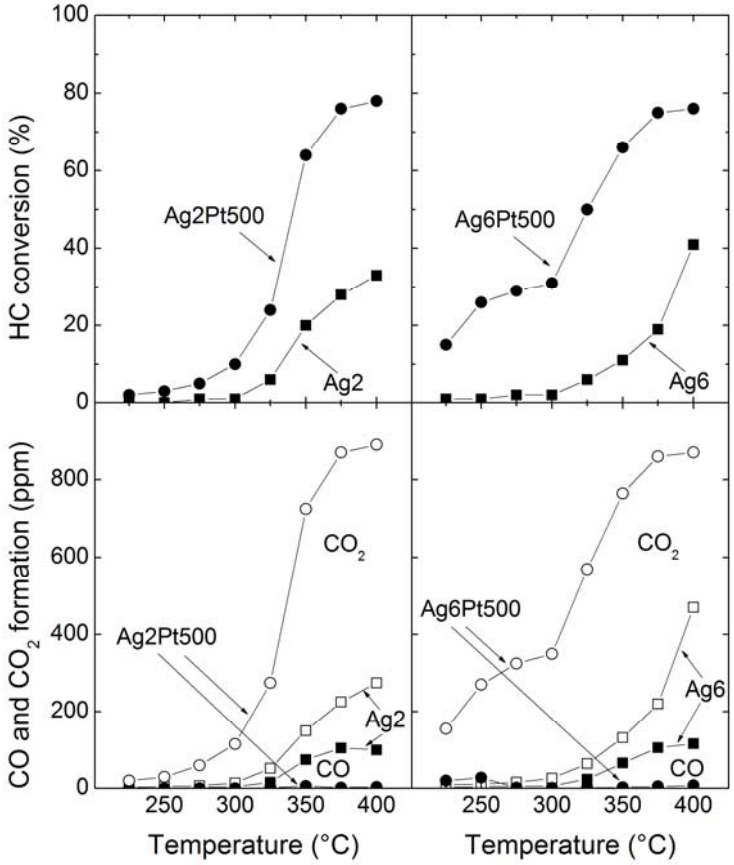

Figure 11: HC oxidation for the Ag2, Ag2Pt500, Ag6 and Ag6Pt500 samples. Top: HC conversion. Bottom: CO and CO_2 formation. Inlet gas composition: 150 ppm n-octane (equivalent to C/N=6 using 200 ppm NO), 1000 ppm H_2, 5 % H_2O, 10 % O_2 with Ar_{bal}. GHSV = 33, 200 h^{-1}.

Although the metals in the present samples may be more or less oxidized, the BEP relation also holds for oxides [76] which ensures that the activation barrier will be lower for the oxidized particles as well. Thus, the relative sticking probability should be higher over Pt species than over the corresponding Ag species. Furthermore, assuming that incorporation of platinum increases the adsorption of hydrocarbons, the Ag2Pt500 sample should be more susceptible to hydrocarbon poisoning compared to the Ag6Pt500 sample, due to its lower number of oxidation sites. The Ag6Pt500 sample will instead reach adsorption/oxidation equilibrium at lower temperatures and hence have a higher overall HC conversion and a higher HC conversion at lower temperatures. Previous studies have suggested that the activity for NO_x reduction over Ag-alumina is affected by many parameters, such as the ratio between oxidation and reduction sites [50], the dissociative chemisorption of hydrocarbons [101, 102] and, in relation to this, the influence of C-C bond strength, steric effects and sticking probability [51]. The promotional effect of the platinum addition to the silver-alumina system could possibly be ascribed to all of these parameters. Pt may change the amount of chemisorbed hydrocarbon on the surface and thereby change the required ratio of red/ox sites for efficient partial oxidation of the hydrocarbon. It may also alter the effective oxidation properties of the surface.

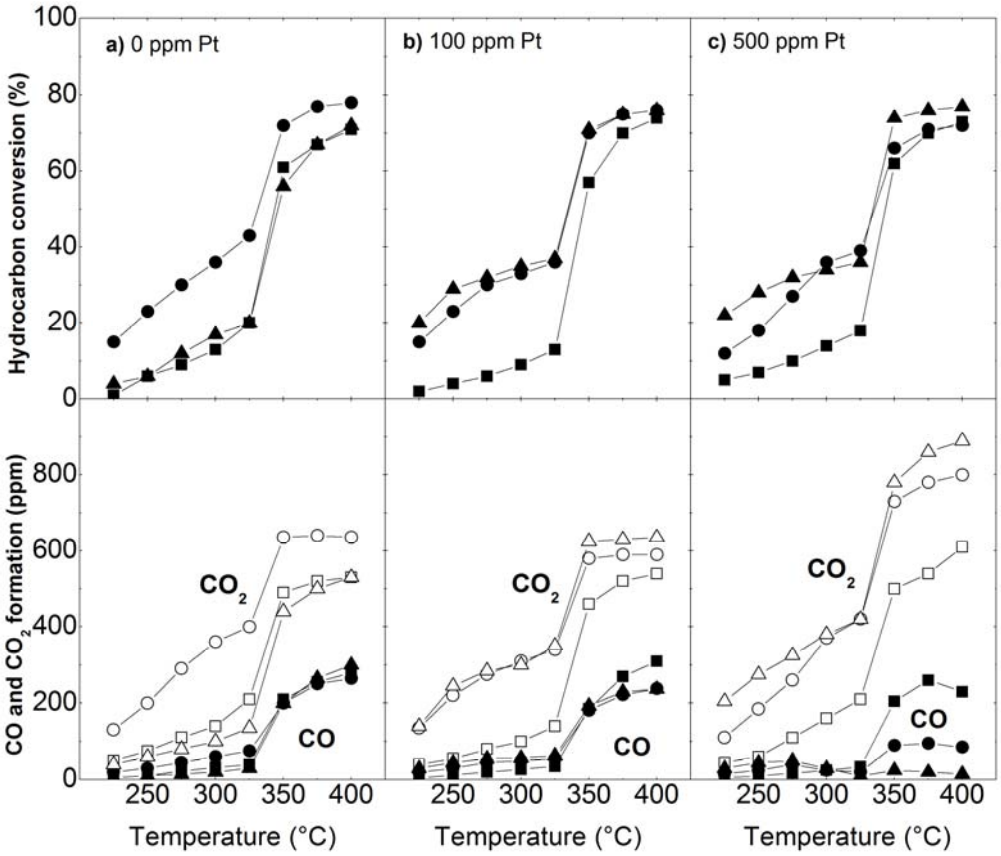

Figure 12: Hydrocarbon conversion (top) as well as CO and CO_2 formation (bottom) from NO_x reduction experiments in flow reactor for 2 wt. % (■), 4 wt. % (●) and 6 wt. % (▲) Ag/Al_2O_3 samples without Pt (left column), with 100 ppm Pt (center column) and with 500 ppm Pt (right column). Inlet gas composition: 200 ppm NO, 10 % O_2, 1000 ppm H_2, 5 % H_2O, Ar_{bal} and n-octane as reducing agent with a C/N molar ratio of 6. GHSV = 33, 200 h^{-1}.

The oxidation, or activation, of the HC is closely related to the reduction of NO_x and to understand the underlying reasons for the increased HC oxidation and NO_x reduction with increasing C-C bond order, many aspects need to be taken into consideration. Steric effects resulting in differences in the hydrocarbon activation/oxidation have been discussed for C−H bond interaction with the catalyst surface. However, in the present case the C−C bond activation is likely more important than the activation of the C−H bond, not necessarily breaking the C−C bond but activating the molecule towards further reactions. The adsorption of the hydrocarbon is also dependent on the shape and orientation of the C−C electron orbitals. The electrons in the π-bonds in ethene and especially ethyne, for which the π-electron cloud has a cylindrical shape, can easily interact with the catalyst surface and thereby form new bonds between the unsaturated hydrocarbon and the surface. Furthermore, the difference in steric hindrance is to a high extent reflected in the sticking probability.

Comparing the hydrocarbon conversions (n-octane) for the Ag2 and Ag6 samples in Figure 11 (no NO_x present) and Figure 12 (NO_x reduction conditions), a higher HC conversion can be seen during the NO_x reduction experiments. The conversion for the Pt-doped samples, Ag2Pt500 and Ag6Pt500, is seen to differ less in response to the presence of NO, however the low temperature HC conversion is higher for the NO_x reduction experiments. The higher HC conversion at low temperature is likely owing to the presence of reactive nitrite species. As the HC conversion is calculated from the CO and CO_2 formation (Eq. 3 and 4), the difference in HC conversion could also be ascribed to the formation of other partially oxidized carbon containing species during the HC oxidation experiments, *e.g.* acetates. Figure 14 shows the NO_x reduction and CO and CO_2 formation during oxidation of C_2 hydrocarbons in the presence of NO and excess O_2 over the Ag2 and Ag6 samples during extinction ramp experiments. The NO_x reduction pattern is generally similar for both

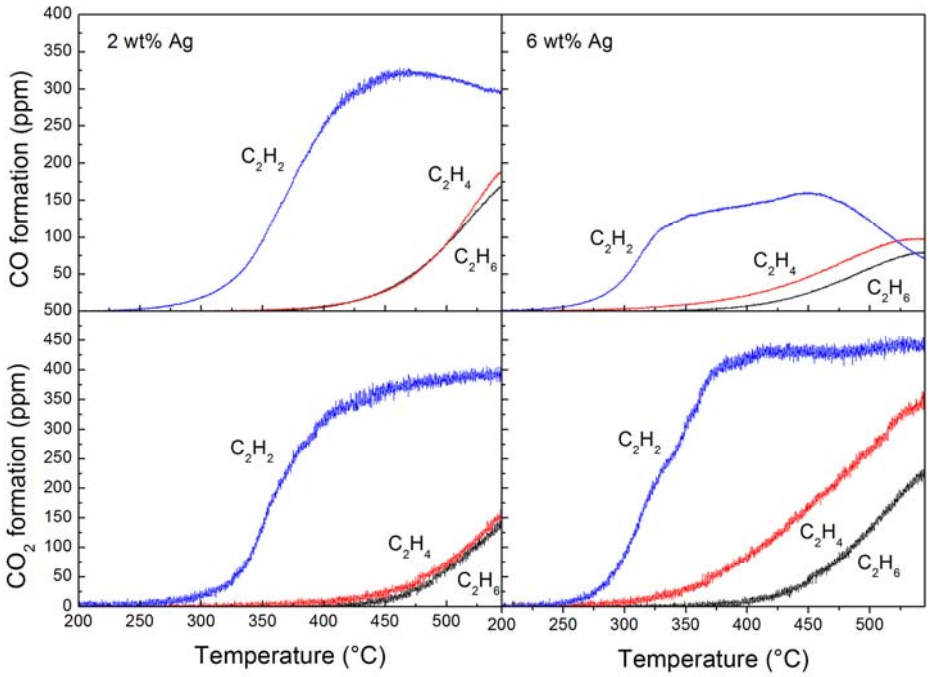

Figure 13: Formation of CO and CO_2 during temperature programmed extinction experiments with C_2H_2 (blue), C_2H_4 (red), and C_2H_6 (black) over Ag2 and Ag6 catalyst. Inlet gas composition: 600 ppm C_2 hydrocarbon, 10% O_2, Ar_{bal}. GHSV: 32, 000 h^{-1}.

catalysts although the temperature windows are shifted to lower temperatures and the maximum NO_x reduction is slightly lower for the Ag6 sample. The highest NO_x reduction is achieved when C_2H_2 is used as reducing agent, over both catalysts, reaching 87% at 412 °C and 82 % at 330 °C for the Ag2 and Ag6 samples, respectively. For both catalysts the C_2H_2 also shows the widest temperature window for NO_x reduction. The maximum NO_x reduction for C_2H_4 and C_2H_6 is 71 and 81%, respectively, over the Ag2 sample and approximately 70%, for both the reductant, over the Ag6 sample. The temperature windows for NO_x reduction with these hydrocarbons are similar, showing no significant activity below 350 and 400°C for the Ag6 and Ag2 samples, respectively.

As the oxidation of the hydrocarbon reductant is of great importance, the work on C_2 hydrocarbons was also extended to include oxygen containing hydrocarbons. The main differences when using oxygenated hydrocarbons are the increase in NO_x reduction and the very low or absent effect of hydrogen addition. The study on oxygenated hydrocarbons was done in combination with non-oxygenated hydrocarbons by using ethanol, EtOH/C_3H_6 and EtOH/gasoline blends as reducing agents (Paper IV) over both powder and monolith coated catalyst samples. The study was performed on both in-house sol-gel prepared samples as well as on a commercial Ag/Al_2O_3 (Catalytic Solutions Inc.). The selection of catalysts also include Pt doped Ag/Al_2O_3 catalysts. The study shows a remarkably high NO_x reduction with a high selectivity towards NH_3. The powder study was used as the basis in the determination of suitable candidates for monolith experiments with more in-depth analysis (Figure 15). The 1500 ppm (C/N=6) EtOH powder experiments showed similar behavior at temperatures up to 400 °C, with 15 °C lower onset temperature for the Ag4 *cf.* CSI and Ag2Pt100.

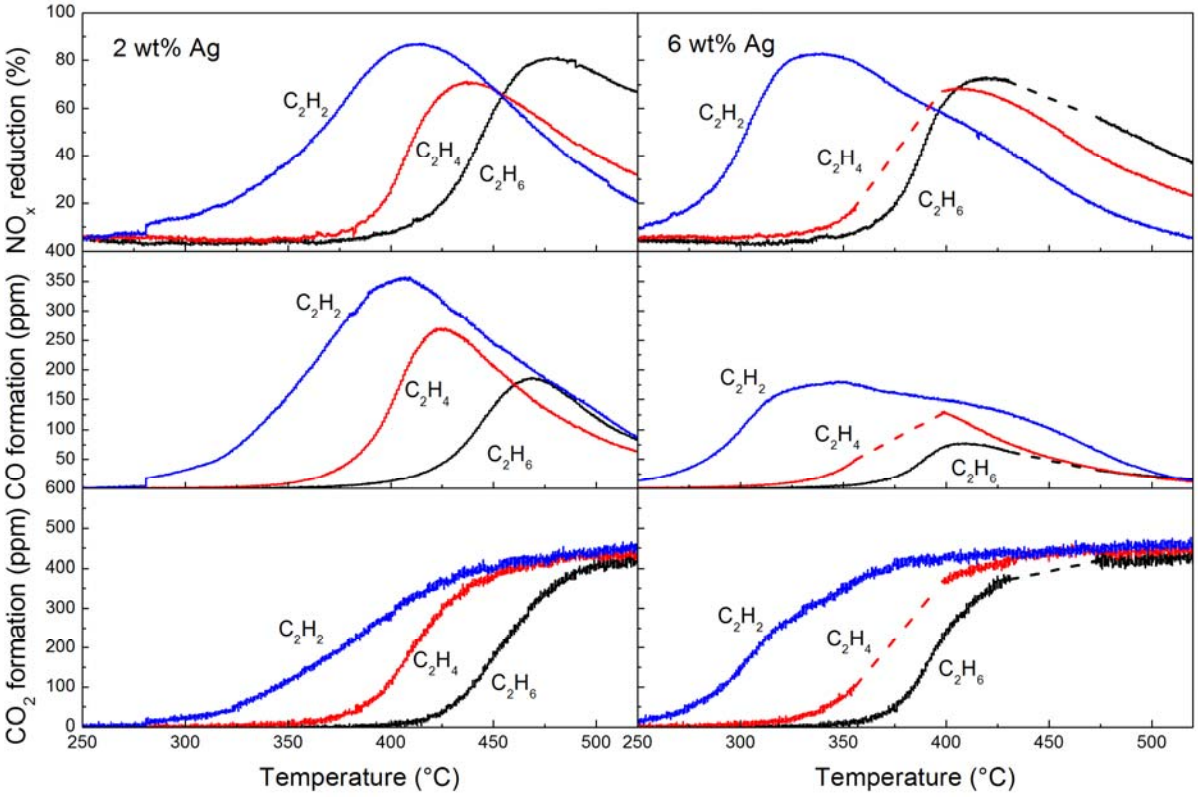

Figure 14: Formation of CO, CO_2 and reduction of NO_x during temperature programmed extinction experiments with C_2H_2 (blue), C_2H_4 (red), and C_2H_6 (black) over Ag/Al_2O_3 catalyst with 6 wt. % (left panel) and 6 wt. % (right panel) nominal silver content. Inlet gas composition: 200 ppm NO, 600 ppm C_2 hydrocarbon, 10% O_2, Ar_{bal}. GHSV: 32, 000 h^{-1}.

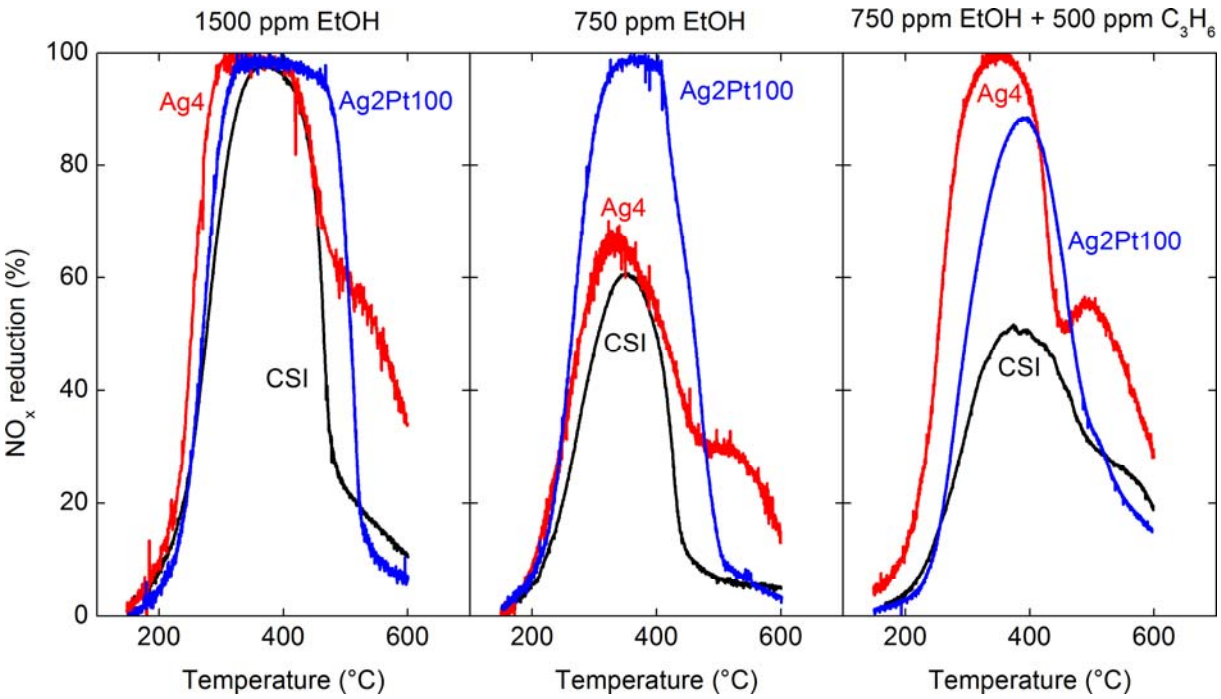

Figure 15: NO_x reduction results from fixed powder bed reactor experiments over CSI (black), Ag4 (red) and Ag2Pt100 (blue) samples. Right panel: 1500 ppm EtOH (C/N=6), middle panel: 750 ppm EtOH (C/N=3) and right panel: 750 ppm EtOH + 500 ppm C_3H_6 (C/N=6) as reducing agent Inlet gas composition: 500 ppm NO, 10 vol. % O_2, 5 vol. % H_2O, and $N_{2,balance}$. GHSV = 50000 h^{-1}.

The temperature window for the Ag2Pt100 extends approximately 70 °C over the other two samples. When the EtOH concentration is decreased to 750 ppm (C/N=3) the Ag2Pt100 sample maintains a high reduction, however at a narrower temperature window, whereas the pure Ag sample, CSI and Ag4, only reach a maximum of 60 % and 65 %, respectively. The reduction is recovered for the Ag4 sample when 500 ppm C_3H_6 is added to the 750 ppm EtOH. The addition of C_3H_6 does however appear to hinder the NO_x reduction for the CSI and Ag2Pt100 samples which display lower reduction compared to when only 750 ppm EtOH was used.

The Ag4 and Ag2Pt100 samples were subsequently wash-coated onto cordierite monoliths and evaluated in a synthetic gas bench reactor, using EtOH/gasoline mixtures as reducing agent (Figure 16). The mixtures are denoted as E(concentration of EtOH), *i.e.* E85 contains 85 % EtOH and 15 % gasoline and all experiments were carried out at a C/N ratio of 6. The results show a much higher NO_x reduction over the Ag4 sample than over the Ag2Pt100 sample, with the Ag4 sample displaying a light-off temperature approximately 50 °C before the Ag2Pt100 sample, contrary to the powder reactor results. In addition, the E85 and E100 results show very similar reduction for the Ag4 sample, whereas the E100 shows strictly higher reductions *cf.* E85 over the Ag2Pt100 sample. The E50 results over the Ag4 sample displays slightly lower reduction at temperatures below 450°C, where after the reduction is high *cf.* E85 and E100. The Ag2Pt100 sample results however, show no improvement at high temperatures when using E50, but instead an overall decrease in NO_x reduction activity is observed. The HC conversion, derived from the formation of CO and CO_2, is almost identical when comparing E100 and E85 for the two catalysts individually. The HC conversion light-off for the Ag4 sample also begins approximately 50 °C before the Ag2Pt100 sample correlating with the NO_x

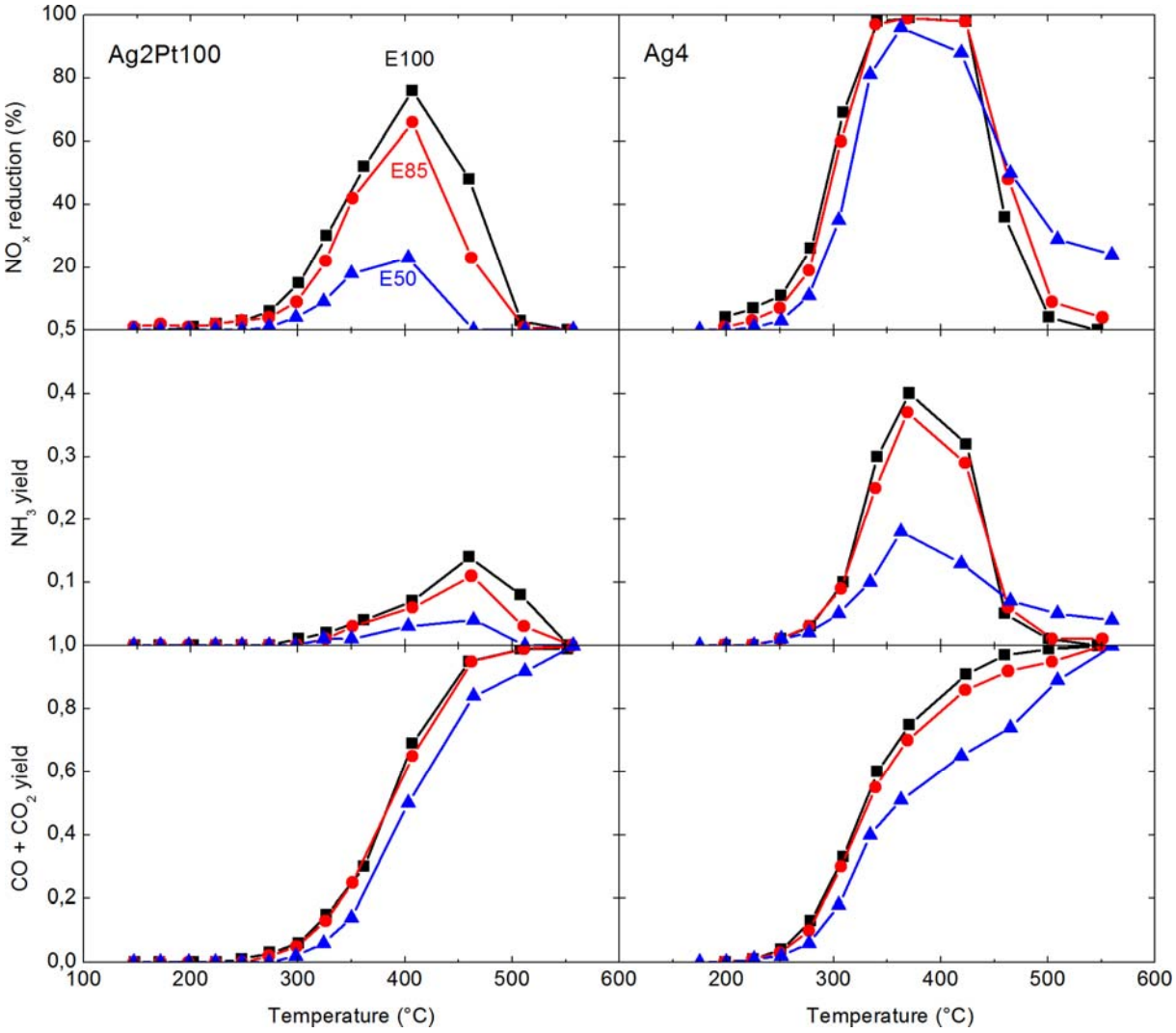

Figure 16: NO_x reduction results (top panels), NH_3 yield (middle panels) and CO + CO_2 yield (bottom panels) from synthetic gas flow reactor experiments for 2 wt. % Ag/Al_2O_3 with 100 ppm Pt (left panels) and 4 wt. % Ag/Al_2O_3 (right panel) using EtOH/gasoline blends as reducing agent. Blends are denoted as E100 (■), E85 (●) and R50 (▲). Inlet gas composition: 500 ppm NO, 10 vol. % O_2, 5 vol. % H_2O, and $N_{2,balance}$. The C/N molar ratio was 6 and GHSV = 35 000 h^{-1}.

reduction light-off. It can be noted that the promotional effect of addition of platinum seen during the powder experiments is not visible for the monolith experiments.

A remarkable result from the EtOH-SCR over Ag/Al_2O_3 catalysts is the NH_3 formation. At low levels the formation of NH_3 is considered as an unwanted byproduct, however at levels of the magnitude showed here it is possibly an asset if the system is used for passive SCR. Combining a system of this type with *e.g.* an ammonia storage catalyst and a NH_3-SCR catalyst could very well result in an interesting system. As stated in the introduction, the addition of a urea tank in light duty vehicles is undesirable due to space limitation, hence NH_3-SCR has been considered as a heavy duty technology only. In addition, one key challenge with HC-SCR is keeping down the fuel penalty derived from the hydrogen reformation of the fuel and the consumption of fuel as reducing agent. As the EtOH-SCR does not require H_2 in order to achieve high reduction, this contribution to the fuel penalty is avoided. If the EtOH-SCR system would be connected to a down-stream NH_3-storage/SCR catalyst, the produced ammonia could be utilized for NO_x reduction. Switching EtOH to the Ag-alumina

catalyst on and off could result in a cycling between HC-SCR, reducing NO_x and charging the NH_3-storage/SCR catalyst, followed by a NH_3-SCR, which consumes the stored ammonia, reducing the fuel penalty even further.

In conclusion, we have shown that the type of reducing agent is a crucial factor when designing a HC-SCR catalyst. The results from using long-chained hydrocarbons such as NExBTL as reducing agent compared with model hydrocarbon such as n-octane vary significantly. The underlying reasons behind this is *e.g.* branching of the hydrocarbon relating to the sticking probability and the C-C bond order relating to both the sticking probability, due to more or less favorable electron orbitals, and also to the partial oxidation, *i.e.* activation, of the HC. Oxidized hydrocarbons such as ethanol display a much higher activity for NO_x reduction compared to for example C_2H_4 even without the presence of hydrogen. When designing a Ag/Al_2O_2 catalyst one must therefore take the intended reducing agent into account.

5.3. Effects of system integration

HC-SCR over Ag/Al_2O_3 has been investigated intensively during the past few decades and numerous papers regarding the effects of alternate synthesis routs, reducing agents, mechanistic surface reactions and the hydrogen effect has been published. The number of applied studies with real exhausts is however fewer. Studying the bridge between laboratory scale experiments and a more applied approach was the final aim of this research project, and the study is presented in Paper V were we attempt to illustrate advantages and difficulties for this type of up-scaled experiments and how they relate to laboratory scale experiments. Initially, the Ag/Al_2O_3 system was investigated in order to ensure that a suitable catalyst was chosen. Papers I-III investigated the effects of silver loading and platinum doping resulting in a deeper understanding of what would be required in engine bench trials. These studies, in combination with a laboratory scale investigation on a synthetic gas bench (SGB, 4.3.1) reactor, indicated that the Ag4Pt100 sample was the most suitable candidate for the up-scaled engine experiments on the pilot-scale reactor (PSR, 4.3.2) setup. In addition to the catalyst itself, the interaction between the catalyst and the reducing agent had to be considered. Not only must the catalyst and reducing agent be compatible, the delivery system must also accommodate the specific reducing agent. Following the work by Kannisto *et al.* [49, 52], Paper II investigated the potential for using a more diesel like hydrocarbon as reducing agent. The Swedish environmental Class 1 (MK1) diesel was initially considered, however due to the composition of the HC the fuel could not be introduced to the system with satisfactory precision. Instead, the commercial biodiesel NExBTL was chosen, as it behaved satisfactory in the reactor system and as it displayed high NO_x reductions (Paper II). In addition, it complied with the project goals of working towards sustainable fuels. The hydrogen effect has also been a research area of great interest since its discovery in year 2000 [43], although few applicable solutions for hydrogen addition in real applications have been proposed. One advantage with the HC-SCR technique is that the system utilizes components already available on the vehicle. If a hydrogen tank would be required this advantage is lost. This study wishes to illustrate the feasibility for onboard applications, requiring a reliable source of hydrogen. For this reason, a Rh/CeO_2-ZrO_2 fuel reformer was added to the system, having shown high reliability and durability in previous studies [103, 104]. The fuel used in the reformer was also the commercial biodiesel NExBTL. The study was done in collaboration with the catalysis group at the Royal Institute of Technology (KTH), Stockholm.

As stated previously, the most promising catalyst candidates from Papers I-III were studied using a SGB setup in lab-scale in order to determine the best candidate for the pilot-scale reactor (PSR) experiments, as well as to ensure an overall functioning system and a functional integration between HC-SCR and the reformer system. The NO_x reduction activity of three HC-SCR catalysts (Ag2, Ag4, Ag4Pt100) was investigated in a synthetic gas bench reactor (SGB) setup, using a hydrogen-rich gas from the fuel reformer at three different H_2 concentrations. As the Ag4Pt100 catalyst showed the largest variation in promotional effect as a function of hydrogen concentration (Figure 19), this catalyst was up-scaled and evaluated in the PSR setup, connected to a one-cylinder diesel engine as the exhaust generator. These experiments were performed using both bottled hydrogen, at three different concentrations, and by using hydrogen supplied from the fuel reformer, at two different concentrations. The HC-SCR catalyst was up-scaled 200 times *cf.* the size of the SGB scale monoliths, allowing the system to process a complete engine exhaust flow with reasonable space velocities. In this setup the HC-SCR catalyst was exposed to real operating conditions using real exhaust gases. The PSR setup enabled comparative experiments between hydrogen originating from bottle and from fuel reformer. One issue that the HC-SCR system shares with the NH_3-SCR system is the need for a well dispersed reducing agent, although not to the same degree. As no decomposition of the hydrocarbon reducing agent is desired, only vaporization, the system will initially not require the same level of complexity. However, as mentioned briefly in the chapter concerning the effects of the reducing agent, the thermal stability of the reducing agent is crucial. During the pilot-scale experiments, a lowered NO_x reduction could be observed related to the C/N ratio. More in-depth studies of the reducing agent later revealed that for some conditions, the temperature in the HC injection zone exceeded 400°C, resulting in a thermal decomposition of the reducing agent (Figure 18). In order to maintain a high reaction temperature in the HC-SCR catalyst, a substantial flow needed to be injected in the DOC, resulting in elevated temperatures in the injection zone. The HC amount which actually reached the HC-SCR catalyst was hence decreased with as much as 50 % resulting in a C/N ratio of approximately 2.

Hydrogen generation

Different ways of introducing hydrogen to the exhaust stream prior to the HC-SCR catalyst has been discussed in both the academic and industrial part of the scientific community. This study therefore utilized a potential onboard hydrogen generator, *i.e.* a fuel reformer. Prior to the integration experiments the aging characteristics of the fuel reformer catalyst was thoroughly investigated in the bench-scale fuel reformer setup, described in detail by Granlund *et al.* with NExBTL [103]. The most important feature for onboard fuel reforming in vehicle applications is the actual amount of hydrogen produced. In addition, the diesel slip, *i.e.* the unconverted fuel passing through the reformer is of great importance, due to fuel penalty considerations.

The main components in the reformate are H_2, CO_2, CO and H_2O, however the presence of by-products are not negligible. These by-products were monitored by the FTIR gas analyzer at similar operating conditions utilized in the SGB experiments. The reformate composition is shown in Figure 17, where the concentrations of the by-products are displayed as C_1-concentrations originating from each HC species in the fuel reformer outlet. A concentration of 2000 ppm C_1 in the reformate corresponds to a concentration of 10 – 40 ppm C_1 in the feed to the HC-SCR catalyst. As the fuel reformer was run at different temperatures for the different operation points *i.e.* hydrogen concentrations, the outlet concentration varied, however HC-SCR active HC-species are present at all temperatures.

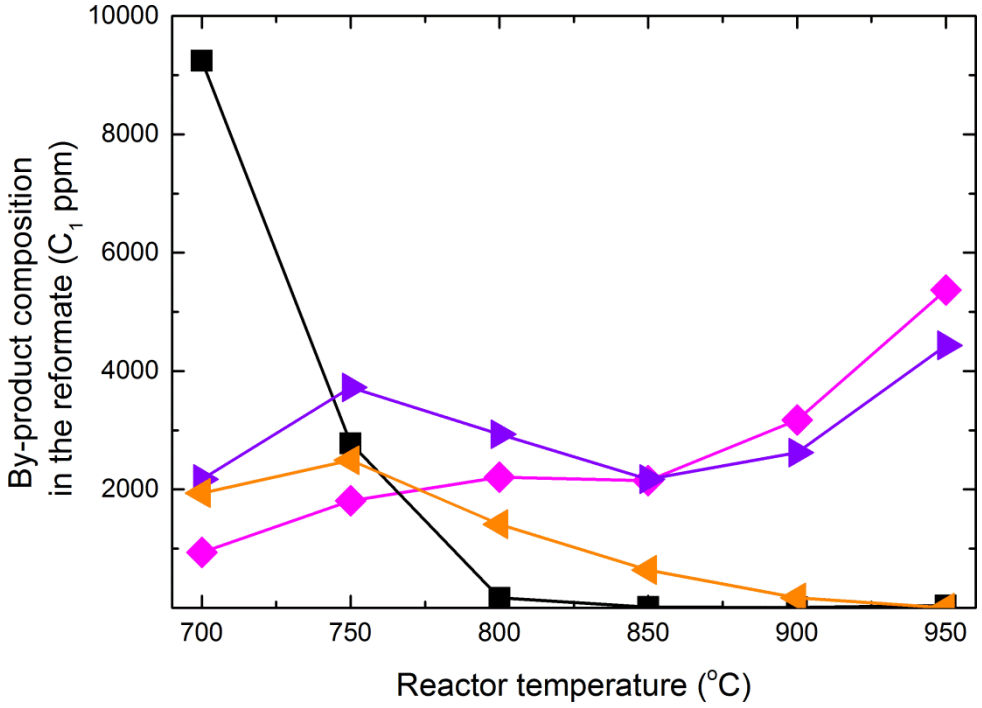

Figure 17: Composition of the reformate at H_2O/C ~2.5 and O_2/C ~0.5 and GHSV ~20,000 h^{-1}. The concentrations of the by-products are displayed as C_1 derived from the different HC species. The species are denoted as: (■) diesel, (◆) CH_4, (◀) propene, and (▶) ethene.

A high activity over the HC-SCR catalyst is relying on an evenly distributed flow of reducing agent, *i.e.* fuel. If the fuel is exposed to high temperature the long hydrocarbon chains will decompose. The decomposition can be either cracking or partial and total oxidation. In the PSR setup, the reducing agent was injected through an air-assisted capillary, mounted right after the DOC. As stated before, the main purpose of the DOC was to heat the exhaust gas stream in order to reach higher reaction temperatures in the HC-SCR catalyst. As a consequence, the reducing agent was exposed to temperatures higher than the reaction temperatures of the HC-SCR catalyst. To fully understand the thermal decomposition of NExBTL, the decomposition was investigated in SGB experiments (Figure 18). The values are presented as percent of total C_1 for each HC species. At temperatures below 300 °C the majority of the hydrocarbons are present as diesel with just a fraction of CO and CO_2. However, the NExBTL starts to thermally decompose slightly above 300 °C. The initial decomposition is followed by a sharp decrease in the diesel fraction and an increase in CO_2 and propane formation, followed by an increase in CO formation. This means that the dominating process, when treating NExBTL thermally is complete oxidation, with CO_2 and water as the main products. More surprisingly is that the methane, ethyne and ethane fractions remain negligible throughout the chosen temperature interval. Neither formaldehyde, nor propene or ethene is formed to a great extent, but remains around 2 %. The temperature at the injection point of the reducing agent did in some cases reach 450 °C. This caused a decrease in the detected diesel signal, at the same time as the signals of the decomposition products increased. This corresponds well with the results from the thermal decomposition experiments. At 450 °C the contribution to total C_1 from diesel is as low as 45 %, meanwhile CO_2 reaches almost 30 % and propane is approximately 20 %.

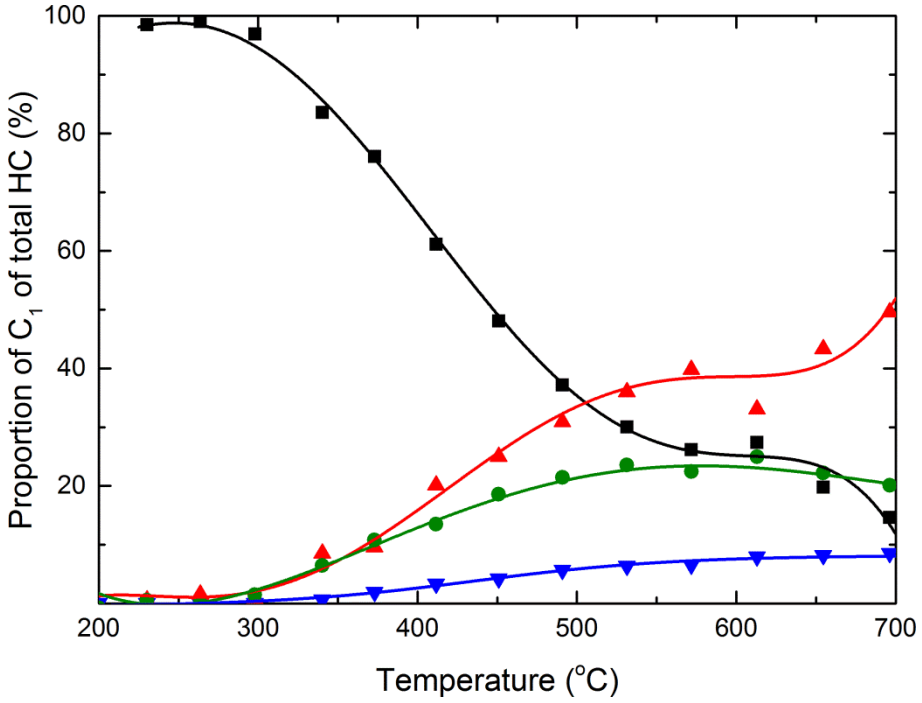

Figure 18: Thermal decomposition of NExBTL in 10 vol. % O_2, 5 vol. % H_2O and $N_{2,\ balance}$. The species are denoted as: (■) diesel, (▲) CO_2, (▼) CO, and (●) propane.

NO_x reduction experiments

In order to compare experiments of the type performed in previous papers (Papers I-IV), the study was performed both using synthetic gas flow reactor and an engine pilot-scale reactor. The SGB experiments were also performed in order to evaluate which of the three HC-SCR catalysts that would be most suitable for up-scaling.

The SGB reactor experiments were performed on three Ag/Al_2O_3 HC-SCR catalysts (Ag2, Ag4 and Ag4Pt100) using hydrogen supplied by the fuel reformer and with NExBTL as reducing agent. The experiments were performed at four hydrogen concentrations 0, 1000, 1500 and 3250 ppm H_2 (Figure 19). The promotional effect from adding hydrogen is clearly seen for all three catalysts. In addition, it can be observed that the effect of adding hydrogen is not proportional to the H_2 concentration. The improvement in NO_x reduction is most prominent at low temperatures and decreases as the temperature increases. The hydrogen effect can be seen over the entire temperature range for the Ag2 catalyst, whereas the effect is negligible for temperatures above 400 °C for both the Ag4 and Ag4Pt100 catalysts (Figure 19). This is likely due to the increased amount of oxidation sites for these two catalysts, oxidizing the majority of the H_2 to H_2O at higher temperatures. The catalyst showing the lowest effect of H_2 for reduction of NO_x at higher temperatures is the Ag4Pt100 sample. Platinum is a well-known oxidation catalyst and at higher temperatures it is likely to consume the H_2 though oxidation to water, preventing it from taking part in the NO_x reduction reactions [16]. At low temperatures however, the largest difference in activity when adding hydrogen is seen for the Ag4Pt100 catalyst. This catalyst also shows the most distinct change in activity as a function of the H_2 concentrations. Hence, the Ag4Pt100 sample was up-scaled and evaluated in the PSR setup equipped with an engine (genset, DX 6000 TE XL C, Yanmar) and a separate fuel reformer for hydrogen production. The Ag4Pt100 HC-SCR catalyst was evaluated, using both bottled hydrogen (Figure 20, top panel) and hydrogen from the fuel reformer (Figure 20, bottom panel). Due to the

complexity of the reactor system concerning the actual total gas flow, which varied with the engine load and other factors, the H_2 concentration could not be chosen with the same accuracy as in the SGB experiments. The hydrogen was therefore introduced at three concentrations from bottle (~1400, ~2800 and ~7000 ppm), and two concentration from the fuel reformer (~1200 ppm and ~2000 ppm). The resulting NO_x reduction displayed was 25, 42 and 53 % at ~236 °C for the bottled hydrogen, respectively, and 16 % at 233 °C and 37 % at 245 °C for the reformate, respectively. The NO_x reduction was calculated by analyzing the total NO_x concentration both upstream and downstream of the HC-SCR catalyst with an FTIR gas analyzer. During the PSR experiments, the C/N ratio was lowered to approximately 4, in order to reduce the adsorption of diesel residues on the HC-SCR catalyst. At higher C/N ratios, a slow decrease in NO_x reduction could be observed over time.

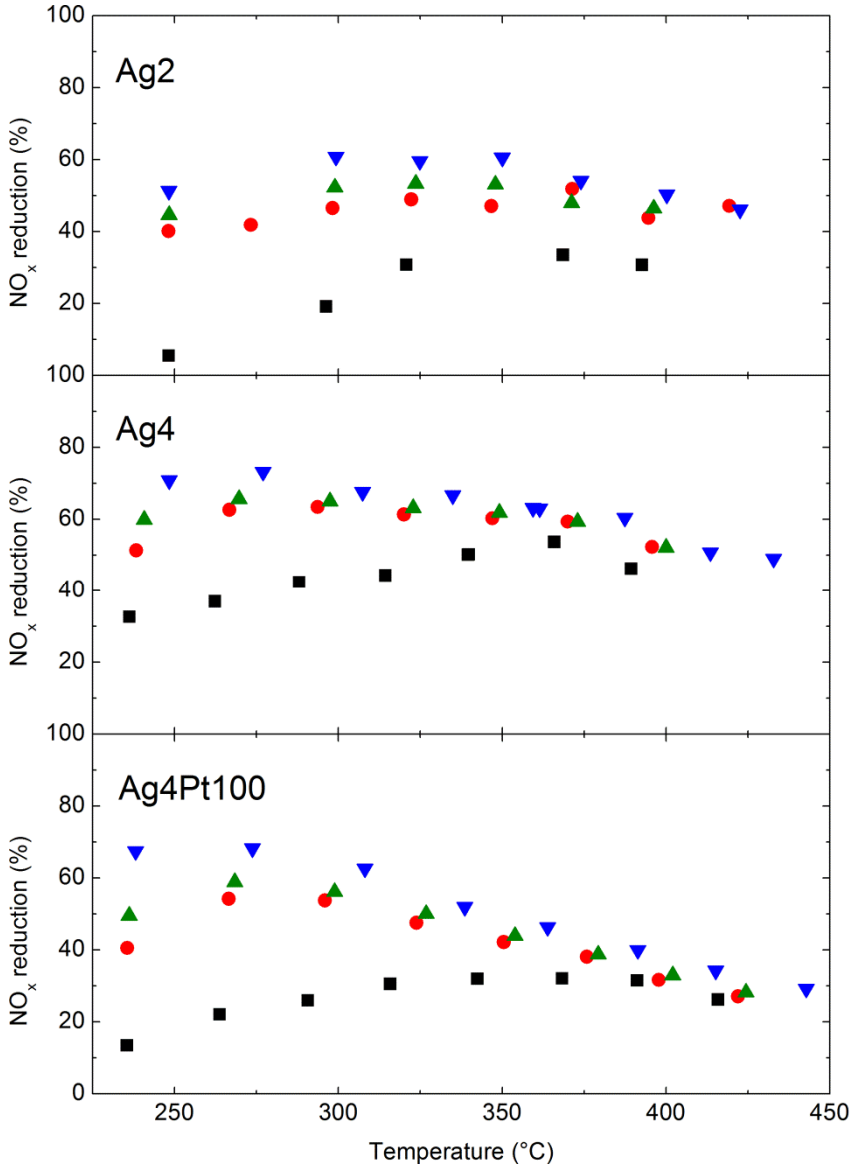

Figure 19: NO_x reduction results from SGB reactor experiments for 2 wt. % (top panel), 4 wt. % (middle panel) and 4 wt. % with 100 ppm(w) Pt (bottom panel) Ag/Al_2O_3 samples. Hydrogen concentrations are denoted as 0 ppm (■), 1000 ppm (●), 1500 ppm (▲) and 3250 ppm (▼). Inlet gas composition: 200 ppm NO, 10 vol. % O_2, 5 vol. % H_2O, and $N_{2,balance}$ with NExBTL as reducing agent. The C/N molar ratio was 6 and GHSV = 33,200 h^{-1}.

When the reducing agent was removed, a decreasing CO and diesel signal could be detected for as long as 15 min. This indicated that carbonate species were adsorbed on the catalytic surface, possibly blocking the active sites, which also has been observed previously [26]. This was also observed when no hydrogen was added to the feed, hence no reliable data could be collected at these conditions. The results from the PSR study show similar trends as the SGB experiments. The NO_x reduction activity is significantly increased with addition of bottled hydrogen at low temperatures and as the temperature is increased the promotional effect is less pronounced (Figure 20, top panel) with no statistical difference above 350 °C. As no data are available for conditions without hydrogen, the actual promotional effect cannot be determined, however when adding 1400 ppm H_2 *cf.* to 7000 ppm H_2 from bottle, the NO_x reduction increases with a factor of two from 25% to 53%. When using hydrogen produced in the fuel reformer, the same trend can be observed, although the promotional effect is present over the entire temperature range. The maximum NO_x reduction activity of up to 55% was achieved using bottled hydrogen (7000 ppm H_2) at temperatures below 325 °C. It should also be noted the when using hydrogen from the fuel reformer, approximately 28% NO_x reduction is reached with 2000 ppm H_2 around 300 °C *cf.* approximately 32% NO_x reduction with 2800 ppm H_2 from bottle. This illustrating the beneficial effect of reformate as compared to bottled hydrogen, likely owing to the HC-SCR active by-product in the reformate.

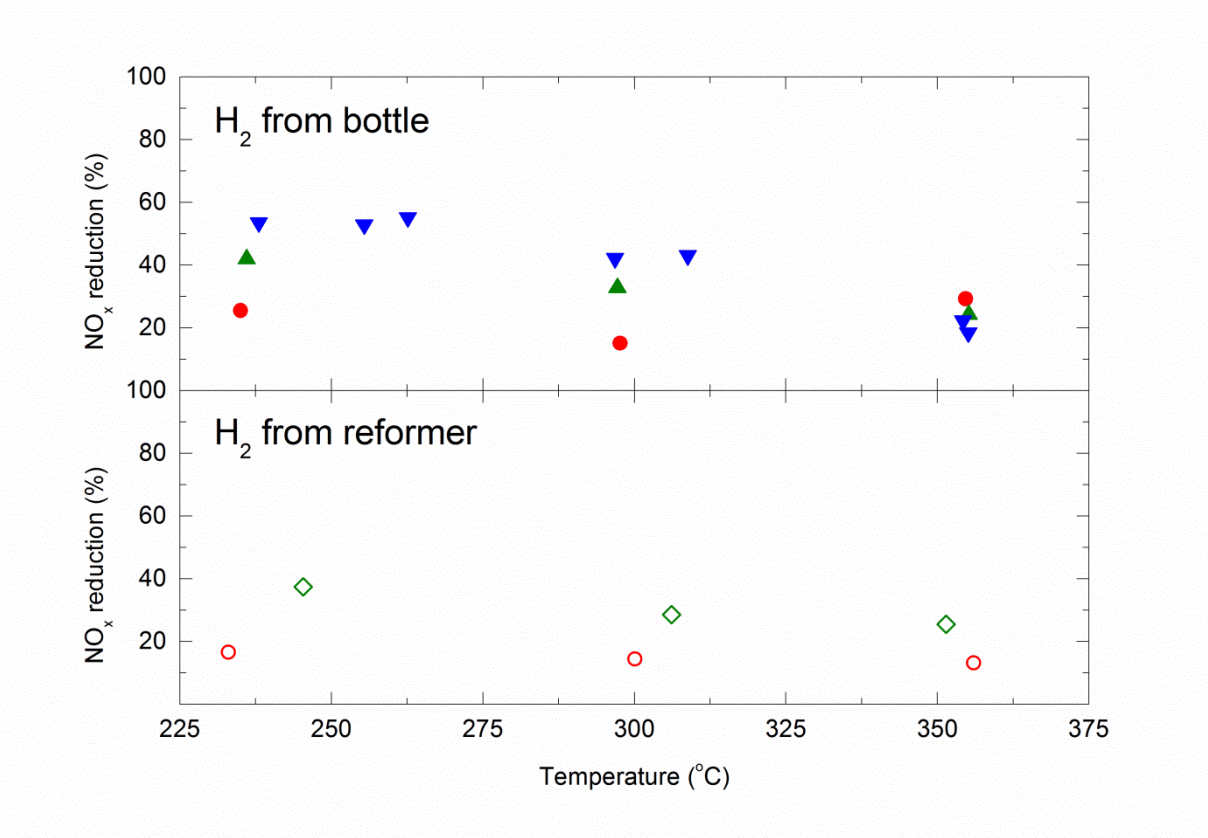

Figure 20: NO_x reduction results from pilot-scale reactor experiments over a 4 wt. % Ag/Al_2O_3 catalyst doped with 100 ppm(w) Pt with bottled hydrogen (top panel) and hydrogen from a fuel reformer (bottom panel). Bottled hydrogen concentrations are denoted as ~1400 ppm (●), ~2800 ppm (▲), ~7000 ppm (▼). Hydrogen was supplied from the fuel reformer at a low concentration (~1200 ppm, ○) and a high concentration (~2000 ppm, ◇). Inlet gas composition: ~420 ppm NO_x, ~10 vol. % O_2, ~5 vol. % H_2O, $N_{2,\ balance}$ and NExBTL as reducing agent with a C/N molar ratio of ~4 and GHSV ~ 22,300 h^{-1}.

6. Conclusions

This work demonstrates high catalytic activity for lean NO_x reduction over the silver alumina catalyst for model hydrocarbons, ethanol and for a commercial biodiesel as the reducing agent for NO_x (Paper I-V). The results show that silver-alumina catalysts, prepared via sol-gel synthesis, display a high consistency regarding surface area, and nature and relative amount of surface silver species, as the silver loading is varied. The samples also display high tolerance towards hydrothermal ageing (Paper I-II). For n-octane, the silver-alumina samples display higher NO_x reduction after ageing up to 650 °C, compared to fresh samples, whilst the activity for lean NO_x reduction decreases after ageing at 700 °C and above. A higher silver loading results in a higher NO_x reduction and a more efficient use of the reducing agent. Additionally, it is shown that the catalytic performance of the silver-alumina sample is stable when subjected to mild hydrothermal treatment (500 °C), which further enhances the efficiency of the reducing agent.

Furthermore, it is concluded that as the samples are doped with trace amounts of platinum, the activity for lean NO_x reduction at low temperatures increases for non-oxygenated hydrocarbons. In addition, it is shown that both the silver loading and the type of reducing agent have a crucial effect on the catalytic performance. A systematic study of the influence of different hydrocarbon reducing agents has been performed, covering C_2 compounds (C_2H_2, C_2H_4, C_2H_6 and ethanol), n-octane and commercial biodiesel (NExBTL). The carbon−carbon bond order (C_2H_2, C_2H_4, and C_2H_6) and silver loading (2 and 6 wt. %) on the formation of partial oxidation products and lean NO_x reduction performance over silver-alumina catalysts is presented. Flow reactor experiments show that the highest activity for the C_2H_x hydrocarbon oxidation and lean NO_x reduction is achieved when C_2H_2 is oxidized in the presence of NO. This is in accordance with the stronger interaction between ethyne and the metal surface, owing to the easily accessible π-electrons, a favorable molecular orientation, and higher sticking probability for C_2H_2 compared to the other C_2 hydrocarbons studied. For the studied hydrocarbons, the temperature window for NO_x reduction is broadened and shifted towards lower temperatures as the C−C bond order increases. Increasing the silver loading from 2 to 6 wt. % is favorable for the oxidizing reactions, leading to activation of both hydrocarbons and NO_x at lower temperatures. Utilizing oxidized hydrocarbons as the reducing agent (ethanol) results in a considerable improvement in NO_x reduction, a lowered onset temperature and a wider temperate window, compared to non-oxygenates, without any addition of hydrogen. The results also show that low-level doping of platinum has little or no beneficial effect on the NO_x reduction for ethanol. When utilizing longer non-oxygenated hydrocarbons however, the addition of platinum is beneficial. The catalyst composition with the highest activity for NO_x reduction, when using n-octane as the reducing agent, is found to be a 2 wt. % Ag/Al_2O_3 sample doped with 500 ppm platinum (Paper I). This catalyst displays the highest low-temperature activity, most likely owing to an increased amount of partially oxidized hydrocarbons on the surface as well as a change in the oxidation potential attributed to the Pt doping. A higher hydrocarbon adsorption could mean that a lower amount of reducing agent would be required for Pt-doped silver-alumina catalysts as compared to the corresponding un-doped samples, which will improve fuel efficiency.

In conclusion, silver-alumina catalysts prepared via the sol-gel method show high activity for NO_x reduction at low temperatures, with high resistance towards hydrothermal ageing. The addition of platinum can be seen to increase the activity for NO_x reduction at low temperatures, particularly for long-chained hydrocarbons. The catalysts are also shown to be compatible with renewable fuels,

although the activity for NO_x reduction is lower for biodiesel as compared to n-octane. Knowledge of the catalytic processes, like the activation of the reducing agent and the NO_x related chemistry, is of major importance for catalyst development. A detailed understanding of these processes will result in better ability to tailor catalysts for *e.g.* future fuels.

7. Acknowledgements

This work has been performed as part of the Mistra (The Foundation for Strategic Environmental Research) funded program E4 (Energy Efficient Reduction of Exhaust Emissions from Vehicles), within the Competence Centre for Catalysis (KCK). KCK is financially supported by Chalmers University of Technology, the Swedish Energy Agency and the member companies: AB Volvo, ECAPS AB, Haldor Topsø A/S, Scania CV AB, Volvo Car Corporation AB and Wärtsilä Finland Oy.

Financial support from Knut and Alice Wallenberg Foundation, Dnr KAW 2005.0055, and Area of Advance Transport are gratefully acknowledged.

I would also like to thank the following persons who have helped in the process of this thesis:

Associate Professor **Hanna Härelind**, my friend and main supervisor, who always takes the time to discuss everything from science to the world in general. Thanks for everything!

Professor **Magnus Skoglundh**, my supervisor and examiner, who always manages to see through the problems and come with great solutions. Thanks for all the help and all the fruitful discussions!

Ph.D. **Hannes Kannisto**, former roommate, friend, gym buddy and fellow beer aficionado, who laid the ground work for the thesis. Thanks for all the help and for making work fell like such a fun place!

Ph.D. **Simon Klacar**, associate professor **Anders Hellman** and associate professor **Henrik Grönbeck**, thanks for all the great discussions and for keeping my ideas within the chemically legal limits.

Ph.D. **Josh Phil** and Ph.D. **Todd Toops**, for making me feel so welcome at ORNL and for all help and great discussions.

Professor **Lars Pettersson** and MSc **Moa Ziethén Granlund** for the great collaboration and all the fun times!

The **EATS group** at Volvo ATR, in particular **Timothy Benham**, **Jan Koegler**, **Mikael Ohlsson**, **Carl Landberg**, **Lennart Andersson** and **Miroslawa Milh**, who put in time and effort, and came with invaluable input and help, is greatly acknowledged.

To all the **colleagues** and **friends** at TYK and KCK for filling the days with interesting discussions and for filling the Friday evenings with great company.

To my **parents, brother** and **sister**, for all the encouragement and support over the years!

To my wonderful fiancée **Emma**, who crossed the sea to brighten my world! Thanks for always believing in me and making my life so great!

8. References

[1] I. Chorkendorff, J. Niemantsverdriet, Concepts of Modern Catalysis and Kinetics. John Wiley & Sons, (2006).

[2] R. Detels, D.P. Tashkin, J.W. Sayre, S.N. Rokaw, F.J. Massey, A.H. Coulson, D.H. Wegman, Am J Public Health, 81 (1991) 350-359.

[3] D. Price, R. Birnbaum, R. Batiuk, M. McCullough, R. Smith, OSTI ID: 549660, PB--98-104631/XAB; EPA--452/R-97/002 TRN: 73221646 PBD: 1997-08-01

[4] C. European Parliament, Regulation (EC) No 715/2007 (2007).

[5] S.i. Matsumoto, CATTECH, 4 (2000) 102-109.

[6] M. Zheng, G.T. Reader, J.G. Hawley, Energy Convers. Manage., 45 (2004) 883-900.

[7] K. Skalska, J.S. Miller, S. Ledakowicz, Sci. Total Environ., 408 (2010) 3976-3989.

[8] W.S. Epling, L.E. Campbell, A. Yezerets, N.W. Currier, J.E. Parks, Cat. Rev. - Sci. Eng., 46 (2004) 163-245.

[9] J. Dawody, M. Skoglundh, S. Wall, E. Fridell, J. Mol. Catal. A: Chem., 225 (2005) 259-269.

[10] UNITED NATIONS FRAMEWORK CONVENTION ON CLIMATE CHANGE, in: U. NATIONS (Ed.), 1992.

[11] G.A. Meehl, W.M. Washington, W.D. Collins, J.M. Arblaster, A. Hu, L.E. Buja, W.G. Strand, H. Teng, Science, 307 (2005) 1769-1772.

[12] L. Hughes, Trends Ecol. Evol., 15 (2000) 56-61.

[13] R.B. Anderson, H. Kölbel, M. Ralek, Vol. 16, New York: Academic Press (1984).

[14] M.E. Dry, Catal. Today, 71 (2002) 227-241.

[15] H. Schulz, Short history and present trends of Fischer–Tropsch synthesis, Appl. Catal. A, 186 (1999) 3-12.

[16] Y. Fernández, A. Arenillas, M. Díez, J. Pis, J. Menéndez, J. Anal. Appl. Pyrolysis, 84 (2009) 145-150.

[17] A. Heinzel, V. Barragan, J. Power Sources, 84 (1999) 70-74.

[18] A.K. Agarwal, Prog. Energy Combust. Sci., 33 (2007) 233-271.

[19] B. Karthikeyan, K. Srithar, Appl. Energy, 88 (2011) 323-329.

[20] T.A. Semelsberger, R.L. Borup, H.L. Greene, J. Power Sources, 156 (2006) 497-511.

[21] M. Stöcker, Angew. Chem. Int. Ed., 47 (2008) 9200-9211.

[22] R. Edwards, V. Mahieu, J.-C. Griesemann, J.-F. Larivé, D.J. Rickeard, SAE Technical Paper, No. 2004-01-1924, (2004).

[23] S. Kim, B. Dale, Int J Life Cycle Ass., 11 (2006) 117-121.

[24] L. Luo, E. van der Voet, G. Huppes, H.A.U. de Haes, Int J. Life Cycle Ass., 14 (2009) 529-539.

[25] E.P. Coelho, C.W. Moles, M.A. dos Santos, M. Barwick, P.M. Chiarelli, SAE Technical Paper, No. 962350, (1996).

[26] S. Kim, B.E. Dale, Bioresour. Technol., 99 (2008) 5250-5260.

[27] H. Halleux, S. Lassaux, R. Renzoni, A. Germain, Int J. Life Cycle Ass., 13 (2008) 184-190.

[28] M. Kapoor, Diesel Emissions Conference India 2011, Platinum Met. Rev., 56 (2012) 36–39.

[29] M. Iwamoto, H. Yahiro, Y. Yu-u, S. Shundo, N. Mizuno, Shokubai, 32 (1990) 430-433.

[30] W. Held, A. Konig, T. Richter, L. Puppe, SAE Technical Paper Series, 900 (1990) 496.

[31] R. Burch, Cat. Rev. - Sci. Eng., 46 (2004) 271-333.

[32] T. Miyadera, Appl. Catal. B, 2 (1993) 199-205.

[33] Y. Itoh, M. Ueda, H. Shinjoh, M. Sugiura, M. Arakawa, J. Chem. Technol. Biotechnol., 81 (2006) 544-552.

[34] C.K. Narula, C.S. Daw, J.W. Hoard, T. Hammer, Int. J. Appl. Ceram. Tec., 2 (2005) 452-466.

[35] R. Burch, P. Fornasiero, T. Watling, J. Catal., 176 (1998) 204-214.

[36] K. Arve, F. Klingstedt, K. Eränen, J. Wärnå, L.E. Lindfors, D.Y. Murzin, Chem. Eng. J., 107 (2005) 215-220.

[37] K. Arve, J.R.H. Carucci, K. Eränen, A. Aho, D.Y. Murzin, Appl. Catal. B, 90 (2009) 603-612.

[38] K. Arve, K. Eränen, M. Snåre, F. Klingstedt, D. Murzin, Top. Catal., 42-43 (2007) 399-403.

[39] R. Burch, J.P. Breen, C.J. Hill, B. Krutzsch, B. Konrad, E. Jobson, L. Cider, K. Eranen, F. Klingstedt, L.E. Lindfors, Top. Catal., 30-31 (2004) 19-25.
[40] X. Shi, Y. Yu, H. He, S. Shuai, H. Dong, R. Li, J. Environ. Sci., 20 (2008) 177-182.
[41] K. Shimizu, H. Kawabata, A. Satsuma, T. Hattori, Appl. Catal. B, 19 (1998) L92.
[42] N. Bion, J. Saussey, M. Haneda, M. Daturi, J. Catal., 217 (2003) 47-58.
[43] S. Satokawa, Chem. Lett., 29 (2000) 294.
[44] J.P. Breen, R. Burch, C. Hardacre, C.J. Hill, J. Phys. Chem. B, 109 (2005) 4805-4807.
[45] J. Breen, R. Burch, Top. Catal., 39 (2006) 53-58.
[46] J. Shibata, K.-i. Shimizu, S. Satokawa, A. Satsuma, T. Hattori, PCCP, 5 (2003) 2154-2160.
[47] K. Arve, H. Backman, F. Klingstedt, K. Eränen, D.Y. Murzin, Appl. Catal. A, 303 (2006) 96-102.
[48] K. Eränen, F. Klingstedt, K. Arve, L.-E. Lindfors, D.Y. Murzin, J. Catal., 227 (2004) 328-343.
[49] H. Kannisto, X. Karatzas, J. Edvardsson, L.J. Pettersson, H.H. Ingelsten, Appl. Catal. B, 104 (2011) 74-83.
[50] H. Kannisto, H.H. Ingelsten, M. Skoglundh, J. Mol. Catal. A, 302 (2009) 86-96.
[51] H. Härelind, F. Gunnarsson, S.M.S. Vaghefi, M. Skoglundh, P.-A. Carlsson, ACS Catal., 2 (2012) 1615-1623.
[52] H. Kannisto, K. Arve, T. Pingel, A. Hellman, H. Harelind, K. Eranen, E. Olsson, M. Skoglundh, D.Y. Murzin, Catal. Sci. Tech., 3 (2013) 644-653.
[53] J. Shibata, Y. Takada, A. Shichi, S. Satokawa, A. Satsuma, T. Hattori, J. Catal., 222 (2004) 368-376.
[54] K.-i. Shimizu, J. Shibata, A. Satsuma, J. Catal., 239 (2006) 402-409.
[55] M.C. Kung, H.H. Kung, Top. Catal., 10 (2000) 21-26.
[56] F.C. Meunier, J.P. Breen, V. Zuzaniuk, M. Olsson, J.R.H. Ross, J. Catal., 187 (1999) 493-505.
[57] K.A. Bethke, H.H. Kung, J. Catal., 172 (1997) 93-102.
[58] C. Shi, M.J. Cheng, Z.P. Qu, X.H. Bao, Appl. Catal. B, 51 (2004) 171-181.
[59] Z. Liu, K.S. Oh, S. Woo, Catal. Surv. Asia, 10 (2006) 8-15.
[60] S. Satokawa, J. Shibata, K.-i. Shimizu, A. Satsuma, T. Hattori, Appl. Catal. B, 42 (2003) 179-186.
[61] H. Backman, J. Jensén, F. Klingstedt, T. Salmi, D.Y. Murzin, Appl. Catal. A, 294 (2005) 49-58.
[62] P. Sazama, L. Čapek, H. Drobná, Z. Sobalik, J. Dědeček, K. Arve, B. Wichterlová, J. Catal., 232 (2005) 302-317.
[63] M. Richter, U. Bentrup, R. Eckelt, M. Schneider, M.-M. Pohl, R. Fricke, Appl. Catal. B, 51 (2004) 261-274.
[64] D. Creaser, H. Kannisto, J. Sjöblom, H.H. Ingelsten, Appl. Catal. B, 90 (2009) 18-28.
[65] R. van Santen, M. Neurock, G. Ertl, H. Knözinger, J. Weitkamp, Handbook of heterogeneous catalysis, 5 (1997).
[66] J. Bergeld, B. Kasemo, D.V. Chakarov, Surf. Sci., 495 (2001) L815-L820.
[67] P.-A. Carlsson, V.P. Zhdanov, M. Skoglundh, PCCP, 8 (2006) 2703-2706.
[68] G. Froment, K. Bischoff, Chem. Eng. Sci., 16 (1961) 189-201.
[69] M.A. Pacheco, E.E. Petersen, J. Catal., 86 (1984) 75-83.
[70] B.P. Chaplin, J.R. Shapley, C.J. Werth, Environ. Sci. Technol., 41 (2007) 5491-5497.
[71] H. Schaper, E. Doesburg, L. Van Reijen, Appl. Catal., 7 (1983) 211-220.
[72] E. Seker, J. Cavataio, E. Gulari, P. Lorpongpaiboon, S. Osuwan, Appl. Catal. A, 183 (1999) 121-134.
[73] A. Gee, B. Hayden, C. Mormiche, T. Nunney, J Chem. Phys., 112 (2000) 7660-7668.
[74] J. Knudsen, N. Martin, E. Grånäs, S. Blomberg, J. Gustafson, J. Andersen, E. Lundgren, S. Klacar, A. Hellman, H. Grönbeck, Phys. Rev. B, 84 (2011) 115430.
[75] A. Hellman, S. Klacar, H. Grönbeck, JACS, 131 (2009) 16636-16637.
[76] A. Vojvodic, F. Calle-Vallejo, W. Guo, S. Wang, A. Toftelund, F. Studt, J.I. Martinez, J. Shen, I.C. Man, J. Rossmeisl, T. Bligaard, J.K. Norskov, F. Abild-Pedersen, J. Chem. Phys., 134 (2011) 244509.
[77] T. Bligaard, J.K. Nørskov, S. Dahl, J. Matthiesen, C.H. Christensen, J. Sehested, J. Catal., 224 (2004) 206-217.

[78] J.N. Bronsted, Chem. Rev., 5 (1928) 231-338.
[79] M.G. Evans, M. Polanyi, J. Chem. Soc. Faraday Trans., 34 (1938) 11-24.
[80] S. Brunauer, Emmet P. H., Teller E., JACS, 60 (1938) 309-319.
[81] M. Bowker, The basis and applications of heterogeneous catalysis, New York: Oxford University Press, (1998).
[82] C. Kittel, Introduction to solid state physics, Hoboken, (2005).
[83] J.F. Moulder, W. F. Stickle, P. E. Sobol, K. D. Bomben, Handbook of X-ray photoelectron spectroscopy. Vol. 40. Eden Prairie, MN: Perkin Elmer, (1992).
[84] B. Imelik, J.C. Védrine, Catalyst characterization: physical techniques for solid materials, Springer, (1994).
[85] P. Atkins, L. Jones, Chemical principles: the quest for insight, Macmillan, (2007).
[86] D.C. Harris, Quantitative chemical analysis, Macmillan, (2010).
[87] D. Kealey, P. J. Haines. "Instant notes." Analytical Chemistry, 270-280, (2002).
[88] J.A. Pihl, T.J. Toops, G.B. Fisher, B.H. West, Catal. Today, 231 (2014) 46-55.
[89] T.J. Toops, J.A. Pihl, Catal. Today, 136 (2008) 164-172.
[90] T.J. Toops, B.G. Bunting, K. Nguyen, A. Gopinath, Catal. Today, 123 (2007) 285-292.
[91] M. Skoglundh, H. Johansson, L. Löwendahl, K. Jansson, L. Dahl, B. Hirschauer, Appl. Catal. B, 7 (1996) 299-319.
[92] N. Bogdanchikova, F.C. Meunier, M. Avalos-Borja, J.P. Breen, A. Pestryakov, Appl. Catal. B, 36 (2002) 287-297.
[93] A.N. Pestryakov, A.A. Davydov, J. Electron. Spectrosc. Relat. Phenom., 74 (1995) 195-199.
[94] V. Bukhtiyarov, V. Kaichev, I. Prosvirin, J. Chem. Phys, 111 (1999) 2169-2175.
[95] A. Manna, B.D. Kulkarni, K. Bandyopadhyay, K. Vijayamohanan, Chem. Mater., 9 (1997) 3032-3036.
[96] F.C. Meunier, J.R.H. Ross, Appl. Catal. B, 24 (2000) 23-32.
[97] L. Rantanen, R. Linnaila, P. Aakko, T. Harju, SAE Technical Paper, No. 2005-01-3771, (2005).
[98] L.-E. Lindfors, K. Eränen, F. Klingstedt, D.Y. Murzin, Top. Catal., 28 (2004) 185-189.
[99] W.-X. Li, C. Stampfl, M. Scheffler, Phys. Rev. Lett., 90 (2003) 256102.
[100] K. Shimizu, J. Shibata, H. Yoshida, A. Satsuma, T. Hattori, Appl. Catal. B, 30 (2001) 151-162.
[101] K. Ruth, R. Burch, R. Kieffer, J. Catal., 175 (1998) 27-39.
[102] K. Arve, F. Klingstedt, K. Eranen, L.E. Lindfors, D.Y. Murzin, Catal. Lett., 105 (2005) 133-138.
[103] M.Z. Granlund, K. Jansson, M. Nilsson, J. Dawody, L.J. Pettersson, Appl. Catal. B, 154 (2014) 386-394.
[104] M.Z. Granlund, O. Görke, P. Pfeifer, L.J. Pettersson, Int. J. Hydrogen Energy, (2014).